Accepted Manuscript

Geochemistry: Exploration, Environment, Analysis

Geochemical footprint of the Millennium unconformity-type uranium deposit, Canada: implications for vectoring new targets

Shannon Guffey, Stephen Piercey, Kevin Ansdell, Tom Kotzer, Gerard Zaluski & David Quirt

DOI: https://doi.org/10.1144/geochem2018-036

Received 13 April 2018
Revised 16 August 2018
Accepted 27 August 2018

GEOCHEMICAL FOOTPRINT OF THE MILLENNIUM UNCONFORMITY-TYPE URANIUM DEPOSIT, CANADA: IMPLICATIONS FOR VECTORING NEW TARGETS

S. Guffey*[1], S. Piercey[1], K. Ansdell[2], K. Kyser[3], T. Kotzer[4], D. Quirt[5], and G. Zaluski[4]**

[1]Department of Earth Sciences, Memorial University, 300 Prince Philip Dr., St. John's, Newfoundland, A1B 3X5, Canada
[2]Department of Geological Sciences, University of Saskatchewan, 114 Science Pl., Saskatoon, Saskatchewan, SN7 5E2, Canada
[3]Department of Geological Sciences and Geological Engineering, Queen's University, Kingston, Ontario, K7L 3N6, Canada
[4]Cameco Corporation, 2121 11th St. W, Saskatoon, Saskatchewan, S7M 1J3, Canada
[5]Orano Canada, 817 45th St. W, Saskatoon, Saskatchewan, S7L 5X2, Canada
**Correspondence (sdg321@mun.ca)*
***Deceased*

Abbreviated title: Millennium U deposit: alteration halo as a vector
Keywords: uranium, unconformity, lithogeochemistry, alteration footprint, element vectoring

ABSTRACT: The Millennium deposit, a *c.* 650-m deep monomineralic uranium deposit, is located in the southeastern Athabasca Basin, Saskatchewan, a region containing numerous high-grade unconformity-type U deposits. 3D modelling of the whole-rock lithogeochemistry of sandstones above the deposit reveals a distinct footprint with select major and trace elements showing increased concentrations towards mineralization. Molar Mg/K ratios increase from background levels 10 km north of the deposit, along the B1 conductive trend, whereas Mo, Co, Rb, and Ga exhibit elevated concentrations immediately above the deposit, extending vertically from the unconformity to surface. Lead, Ag, Bi, Sb, REE, and Y exhibit elevated concentrations up to 650 m above the main mineralized body. Increasing Mg/K values indicate the transition from diagenetic to hydrothermal alteration with shifts from illitic (K-dominant) to chloritic and dravitic (Mg-dominant) alteration, with the latter increasing more proximal to mineralization. Trace element enrichment patterns highlight that fractures and faults were conduits for fluid flow from the basement into the basin, both during ore formation and through tectonically driven post-depositional remobilization. Key indicators such as molar element ratios (Mg-K-Al) and trace elements related to redox reactions provide scalable vectors at the Millennium deposit that are likely applicable to similar unconformity-type U deposits elsewhere.

KEYWORDS: *Millenium deposit; uranium; unconformity-type; 3D modelling*

The Athabasca Basin, located in northern Saskatchewan and Alberta, hosts high-grade unconformity-type U deposits that are important contributors to global U production (Fayek &

Kyser 1997; Cuney 2005; Hiatt & Kyser 2007). The Millennium deposit, located in the southeastern Athabasca Basin, contains 75.9 Mlbs. $U_3O_{8,}$ at a grade of 2.4% U_3O_8, (indicated resources); 29.0 Mlbs. $U_3O_{8,}$ at a grade of 3.2% U_3O_8 (inferred resources); and occurs at *c.* 650 m depth (Cameco Corporation 2015). The mineralization is primarily located in the variably altered Archean/Paleoproterozoic crystalline basement rocks, with approximately 20% present at the unconformity.

Unconformity-type U deposits occur at or near an unconformity between a Paleo- to Mesoproterozoic, redbed sedimentary basin and an Archean to Paleoproterozoic, metasedimentary basement (Tremblay 1982; Cuney 2009; Kyser 2014). Mineralization is a redox reaction product of hydrothermal, oxidized brines carrying dissolved U interacting with a reductant at the site of deposition (diagenetic-hydrothermal metallogenic model: Hoeve & Quirt 1984; Cuney 2009; Kyser 2014). The source of U and the fluids has been interpreted to be the sedimentary basin, the basement, or both (Hoeve & Sibbald 1978; Fayek & Kyser 1997; Hecht & Cuney 2000; Madore *et al.* 2000; Richard *et al.* 2010); most authors agree that the genetic model involves convection- and tectonic-driven hydrothermal fluid transport of oxidized sandstone brine interacting with reduced basement fluids, reduced basement gases, or with reduced basement lithologies, leading to deposition of uranium oxides (Hoeve & Sibbald 1978; Hoeve & Quirt 1984; Kotzer & Kyser 1995; Schaubs *et al.* 2005; Cui *et al.* 2012; Kyser 2014; Dargent *et al.* 2015; Li *et al.* 2016; Pascal *et al.* 2016). Deposits are generally described as two styles: 'unconformity-contact' and 'basement-hosted' in reference to their location (Hoeve & Quirt 1984; Fayek & Kyser 1997). Uranium mineralization in the Athabasca Basin typically forms through a coupled redox reaction involving uranyl (U^{6+}) and ferrous (Fe^{2+}) species (McGill *et al.* 1993; Alexandre *et al.* 2005; Ng *et al.* 2013b).

The hydrothermal processes associated with mineralization affect the basin sandstones to varying degrees, leaving a geochemical signature that changes with proximity to a deposit, therefore creating the potential for vectoring toward mineralization (Hoeve & Quirt 1984; Earle & Sopuck 1989; Kyser & Cuney 2008). These alteration haloes in the basinal sandstones, often many times larger than the deposit itself, are dominated by illite, kaolinite, chlorite, and dravite; and display quartz dissolution and loss of diagenetic hematite ('bleaching') (Hoeve & Quirt 1984; Zhang *et al.* 2001). Complex (polymineralic) uranium mineralization, usually associated with the unconformity-contact style of deposit, contains varying amounts of sulfides and arsenides that contain pathfinder elements such as Ni, Co, Cu, Mo, Pb, and Zn, whereas simple (monomineralic) mineralization, such as at Millennium, is usually found in basement-hosted deposits and lacks, or contains only minor amounts of, pathfinder-providing sulfides and arsenides (Hoeve & Sibbald 1978; Sopuck *et al.* 1983; Fayek & Kyser 1997; Jefferson *et al.* 2007; Kyser & Cuney 2008; Chi *et al.* 2013; Ng *et al.* 2013a; Li *et al.* 2016). The clean sandstones in the eastern Athabasca Basin are ideal for the characterization of vectoring haloes, as they are unmetamorphosed, supermature quartz arenites with monomictic quartz pebble beds and minor siltstone beds (Hiatt & Kyser 2007; Ramaekers *et al.* 2007). Against an average rock SiO_2 content of 95% in the eastern Athabasca Group Manitou Falls Formation sandstones (Quirt 1985), background values of other major and trace elements are low and uniform, making subtle anomalies detectable. Therefore, we propose that the influence of hydrothermal mineralization is identifiable above the deposit at the unconformity, even if weak, and can be mapped in three dimensions as a function of distance from the source with GIS-based software.

The Millennium deposit is monomineralic and deep at *c.* 650 m below the surface and *c.* 100–150 m below the unconformity; however, it is well explored, and the overlying sandstones

can be evaluated for the distal lithogeochemical footprint and its variation with proximity to the deposit. A legacy database of >3000 samples over a 20-km strike length was made available by Cameco Corporation for in-depth data analysis, supporting a comprehensive study capable of capturing subtle variations not seen from a more targeted exploration objective. To avoid undue influence from high-grade mineralization, only samples with U concentrations <1000 ppm were included in the study. By examining the sandstone geochemistry and host-rock alteration mineralogy of these samples, the footprint of the deposit related to the ore forming processes can be characterized; this is typically much larger in scale than the footprint related to the mineralization itself and can provide vectoring capabilities. These characteristics may then be applied to future exploration efforts in the attempt to locate other unconformity-contact deposits at great depth, or perhaps basement-hosted deposits with some presence at the unconformity; often smaller in size, but preferable for extraction due to their simple mineralogy and superior strength and competency of wall-rocks (Alexandre *et al.* 2005; Roy *et al.* 2006; Jefferson *et al.* 2007; Kerr & Wallis 2014). The aim of this paper is to assess potential vectors toward mineralization through examination of the sandstone lithogeochemical footprint associated with host-rock alteration, variably elevated U contents, and the lithostratigraphy of the sandstone above the deposit.

Regional geology

The Millennium deposit is located in the southeastern Athabasca Basin, a *c.* 1.71–1.54 Ga sandstone basin that unconformably overlies the 2.9–1.8 Ga basement of the Rae and Hearne provinces, and the Taltson Magmatic Zone of the Canadian Shield (Fig. 1a, Armstrong & Ramaekers 1985; Kyser *et al.* 2000; Card *et al.* 2007; Rainbird *et al.* 2007; Creaser & Stasiuk

2007; Alexandre *et al.* 2009; Jeanneret *et al.* 2016, 2017; Card *et al.* 2018). The Rae and Hearne provinces were juxtaposed along the Snowbird Tectonic Zone, prior to accretion of Paleoproterozoic rocks of the Reindeer Zone to the eastern margin of the Hearne Province during the development of the Trans-Hudson Orogeny (Hoffman 1988; Ansdell 2005; Corrigan *et al.* 2009).

The Hearne Province underlying the eastern Athabasca Basin includes the Mudjatik and Wollaston domains (Lewry & Sibbald 1980; Hoffman 1988). The Mudjatik Domain consists of mainly Archean felsic gneisses with lesser Archean and Paleoproterozoic supracrustal rocks, and the Wollaston Domain contains Archean granitoid gneisses and overlying Paleoproterozoic metasedimentary rocks (Annesley *et al.* 2005a; Yeo & Delaney 2007). The majority of the U deposits found throughout the eastern Athabasca are situated along the transition between the Mudjatik and Wollaston domains, a 20-km wide corridor known as the Wollaston-Mudjatik Transition Zone (WMTZ) (Fig. 1b; Annesley *et al.* 2003; Annesley *et al.* 2005a; Jeanneret *et al.* 2016). The WMTZ represents the transition between differing deformation styles, metamorphism, structure, and lithology in the two domains, defined by the shift in fabric from linear and NE-trending (Wollaston Domain) to curvilinear (Mudjaktik Domain) (Lewry & Sibbald 1980; Annesley *et al.* 2005a; Jeanneret *et al.* 2016).

The Athabasca Basin contains dominantly quartz arenitic sedimentary fill that formed through rapid tectonic uplift and thermal subsidence (Hiatt & Kyser 2007; Rainbird *et al.* 2007). The rocks of the Rae and Hearne provinces were weathered before the sandstones were deposited, as an interpreted regolith underlies the basal contact of the basin (Hoeve & Sibbald 1978; Macdonald 1985). The Athabasca Group contains four major sedimentary sequences of mainly fluvial, lacustrine, and aeolian material with minor marine detritus in the uppermost units.

Generally, the sequences fine upwards; all are sandstone-rich except for the final, marine sequence, which contains more shales and carbonates (Ramaekers & Catuneanu 2004; Hiatt & Kyser 2007). The Millennium deposit is located below the Manitou Falls Formation, a sandstone-conglomerate formation with high quartz content deposited in an alluvial fan to braided stream environment (Ramaekers *et al.* 2007; Hiatt & Kyser 2007). The lack of feldspar and other minerals, along with the presence of clay minerals, suggests that the source rocks were heavily altered through weathering and transport, dominantly east to west, and later diagenesis (Hiatt & Kyser 2007). Fluid inclusion and clay mineralogy studies suggest that the original depth of the basin was up to 5–6 km, although currently sedimentary cover is 1–2 km thick (Pagel *et al.* 1980; Hoeve *et al.* 1981).

Compressional and extensional regimes affected the basement rocks of the Hearne province both prior to and after the development of the Athabasca Basin (Annesley *et al.* 2005a, Jeanneret *et al.* 2016). These tectonic events were essential for the genesis of uranium mineralization, as they reactivated basement structures that created the faults and fracture zones that served as fluid conduits between the basement and basin rocks and were the driving mechanism for fluid flow across the unconformity (Cui *et al.* 2012; Chi *et al.* 2013).

Deposit geology

Basement geology

The Millennium U deposit is located along the B1 trend, a conductive NNE-trending structural corridor within the WMTZ that contains multiple faults and extensive alteration (Roy *et al.* 2006). The basement rocks are complexly folded by two main deformation events (D_1 and D_2) into a series of doubly-plunging, tight, upright to overturned, NE-trending folds with

moderately to steeply dipping axial planes. The Wollaston Group rocks at the Millennium deposit lie in a north-trending overturned D_2 synform (Roy *et al.* 2006). The Mother fault, a major reverse fault with a northerly strike and moderate easterly dip, lies in the footwall of the deposit (Fig. 2a; Cloutier *et al.* 2009). It contains pre-ore quartz within *c.* 10 m thick fault breccia hosted in a clay matrix (Roy *et al.* 2006; Cloutier *et al.* 2009). The deposit is hosted in a complex fault zone *c.* 20–100 m above the Mother fault.

The basement rocks are a complex assemblage of calc-silicate-bearing rocks, graphitic and non-graphitic pelitic to semi-pelitic gneisses and schists, pegmatites, and leucogranites (Fig. 2a; Roy *et al.* 2006; Cloutier *et al.* 2009). Zircon and monazite ages for Archean granitic gneiss and Hudsonian granitic pegmatite (U-Pb) has given an approximate crystallization age of 2.7 Ga with a major overthrusting event at *c.* 1.8 Ga (Annesley *et al.* 2007). The host rock assemblage contains intensely altered and brecciated graphitic lithologies and replacement and fracture-filling vein U mineralization. Structural reactivation at *c.* 1.35 Ga (Annesley *et al*. 2007) resulted in elevated permeability of the fault zone, which allowed significant fluid flow into the basement in what is interpreted as a dilatant portion of the fault system (Roy *et al.* 2006; Cloutier *et al.* 2009; Fayek *et al.* 2010). The rocks below the Mother fault are not well explored but contain non-graphitic semipelitic and granite gneisses (Roy *et al.* 2006; Cloutier *et al.* 2009).

Athabasca Group

Along the B1 trend, the Athabasca Group sandstones, unconformably overlying the basement rocks, consist of 500–700 m of the Manitou Falls Formation, thickening toward the northern end of the trend (Roy *et al.* 2006; Hiatt & Kyser 2007). The Manitou Falls Formation is subdivided into four lithofacies (MFa, MFb, MFc, and MFd) with gradational, conformable contacts (Roy *et al.* 2006; Hiatt & Kyser 2007; Ramaekers *et al.* 2007). The oldest lithofacies,

the MFa, directly overlies the sub-Athabasca unconformity. It is fine- to coarse-grained with disseminated pebbles and rare intercalated siltstones and mudstones, with a maximum thickness of 100 m (Yeo *et al.* 2002; Roy *et al.* 2006; Ramaekers *et al.* 2007). The MFb is medium- to coarse-grained quartz arenite, approximately 150 m thick, with local intercalated siltstone and clast-supported conglomerate beds. The MFa and MFb lithofacies typically contain diagenetic purple specular hematite and heavy mineral bands and are slightly radioactive due to the presence of Th-bearing aluminum phosphate-sulfate (APS) minerals that have replaced detrital monazite, which are overprinted by pink to red hematite (Hoeve & Quirt 1984; Roy *et al.* 2006; Mwenifumbo & Bernius 2007). The MFc is <100 m thick and consists of medium- to coarse-grained quartz arenite with <1% clay. The MFd is up to 200 m thick and consists of fine- to medium-grained sandstone with >1% clay intraclasts; in the study area, it lies beneath 0–39 m of glacial overburden (Yeo *et al.* 2002; Roy *et al.* 2006; Ramaekers *et al.* 2007).

Uranium mineralization

The majority of mineralization at Millennium is located in the basement, more than 650 m below the surface and over *c.* 100 m below the unconformity (Fig. 2c; Roy *et al.* 2006; Cloutier *et al.* 2009); however, *c.* 20% is present at the unconformity (Fig. 2b). It is monomineralic, consisting of mostly pitchblende with minor coffinite (Roy *et al.* 2006; Cloutier *et al.* 2009; Fayek *et al.* 2010). Styles of mineralization are diverse and range from massive replacement, which is the dominant style; to matrix replacement in breccia and fracture fills, veins and veinlets, blebs and aggregates; to fine disseminated grains (Roy *et al.* 2006; Cloutier *et al.* 2009; Fayek *et al.* 2010). Mineralization is localized in a 25–55 m thick unit of pelitic-semipelitic gneisses and schists (the *Host Assemblage;* Fig. 2a). Ore-grade mineralization is concentrated within a reverse fault in the hanging wall of the basement beneath the *Graphitic*

Marker unit (Roy *et al.* 2006). Weaker mineralization is found both below and above this unit and occurs in various lithologies including calc-silicates, pelitic to semipelitic gneisses and schists, and graphitic metasedimentary rocks (Roy *et al.* 2006). At the unconformity, massive to semi-massive to densely disseminated monomineralic pitchblende replaces the sandstone and basement rocks immediately below. Textures here include clasts of pitchblende in a pitchblende matrix, massive replacement, infilling of pore space between sand grains, and thin veinlets (Zaluski, pers. comm. 2016). Mineralization at the unconformity extends downdip into the mineralization located in the basement rocks along the upper reverse fault system, and grades are similar for both the unconformity and basement styles (Zaluski, pers. comm. 2016).

Uranium-Pb and Pb-Pb geochronology on uraninite in eastern Athabasca uranium deposits has produced ages that vary from circa 1.6 to 0.2 Ga, with age peaks that appear to correspond to far-field orogenic events that may have sparked fluid flow along reactivated structures, e.g., the Mazatzal and Grenville orogenies, the 1.27 Ga Mackenzie Dike Swarm, the 1.1 Ga Moore Lakes gabbro-diabase, and the breakup of Rodinia (Fayek & Kyser 1997; Alexandre *et al.* 2009; Cloutier *et al.* 2009; Mercadier *et al.* 2009; Fayek *et al.* 2010; Annesley *et al.* 2017, among others). Apparent dates on the mineralization at Millennium range from 1.75–0.28 Ga (Cloutier *et al.* 2009; Annesley *et al.* 2007; Mercadier *et al.* 2009; Fayek *et al.* 2010). The oldest are model Pb-Pb ages from disseminated uraninite grains, which range from 1.75–1.65 Ga, and suggest that the basement was one of the potential U sources (Fayek *et al.* 2010). Cloutier *et al.* (2009) obtained a regressed chemical age for "unaltered" uraninite of 1.59 Ga, which is interpreted as the main mineralization event at Millennium; this corresponds to the interpreted primary mineralization event observed in many locations in the Athabasca Basin (Alexandre *et al.* 2009). Younger age groupings obtained with the Pb-Pb and Ar-Ar systems

range from 1.4–1.2 Ga and 1.1–0.8 Ga (Cloutier *et al.* 2009; Fayek *et al.* 2010). Using electron microprobe and ion microprobe analyses, U-Pb age clusters were identified on uraninite from the massive replacement and veins at 1.35–1.25 Ga, 1.2–0.9 Ga, 0.75–0.55 Ga, and 0.3 Ga (Annesley *et al.* 2007; Mercadier *et al.* 2009). These younger dates are associated with resetting or Pb-loss events that are temporal with far-field tectonic events (Kotzer & Kyser 1995; Fayek & Kyser 1997; Annesley *et al.* 2007; Alexandre *et al.* 2009; Cloutier *et al.* 2009; Fayek *et al.* 2010).

Host-rock alteration

At the Millennium deposit, both diagenetic and hydrothermal alteration are present, with hydrothermal alteration intensifying proximal to mineralization (Roy *et al.* 2006; Cloutier *et al.* 2009; Fayek *et al.* 2010). The alteration types and temperatures suggest that the dominant fluids responsible for alteration were basinal brines before and after interactions with basement rocks (Cloutier *et al.* 2009); fluid inclusion data support this hypothesis and suggests late remobilization of materials by meteoric waters (Fayek *et al.* 2010).

Basement alteration

Alteration in the basement occurs as B enrichment combined with Na_2O and Zn depletion and is chiefly present in the structural hanging wall to the Mother fault; the lithologies below the Mother fault have not been sufficiently explored to fully characterize the alteration therein (Roy *et al*. 2006). Cloutier *et al.* (2009) grouped the alteration into pre-ore, syn-ore, and post-ore phases, showing a progressive decrease in temperature. Pre-ore alteration (350–250º C) is a retrograde metamorphic alteration of biotite to chlorite and Fe-Ti oxides in the metapelitic assemblages, overprinted by fine- to medium-grained illite ('muscovite' of Cloutier *et al.* (2009)). The syn-ore alteration includes illite, hematite, and rare fine-grained APS minerals

associated with uraninite. Syn- to post-ore alteration includes fine-grained dravite in a breccia matrix and quartz-dravite veinlets, with calcite and pyrite veins cross-cutting dravite veins. Later phases of fine-grained chlorite and minor pyrite fill void spaces formed through earlier alteration, with late-stage chlorite alteration (185–175º C) present in the upper reverse fault (Cloutier *et al.* 2009).

Roy *et al.* (2006) documented three alteration zones over *c.* 150 m in the basement rocks (Fig. 2b): 1) distal alteration both above and below the Mother fault characterized by saussurite and sericite of probable retrograde metamorphic origin; 2) a proximal halo of chlorite and illite with local hematite that surrounds the graphitic Marker Unit; and 3) a central halo of illite-dravite between the proximal halo and the Mother fault. Uranium mineralization is located in the proximal halo, associated with chlorite alteration (Roy *et al.* 2006). Argillic alteration of feldspar and mica in the host rocks ranges from weakly-developed in unmineralized lithologies to strongly-developed (locally complete clay replacement) with strong mineralization (Fayek *et al.* 2010).

Sandstone alteration

Manitou Falls Formation sandstones have been diagenetically and hydrothermally altered, producing variable clay mineral species and abundances. Regionally, the Millennium and several other unconformity-type U deposits (e.g., Key Lake, McArthur River), are located within a major semi-regional illite-chlorite-dravite-silicification anomaly within dickite-dominated background sandstones (Fig. 1b; Hoeve & Quirt 1984; Earle & Sopuck 1989; Quirt & Wasyliuk 1997; Quirt 2001). Above the Millennium deposit, the sandstones exhibit strong bleaching and quartz dissolution, and increasing clay mineral contents with increasing depth (Roy *et al.* 2006). The upper and lower lithofacies contain hydrothermal illite ± chlorite ± kaolinite ± dravite,

whereas the middle sandstones are dominated by dickite (Roy *et al.* 2006). The alteration paragenesis at the deposit described here is based primarily on Cloutier *et al.* (2009), and is similar to that reported in other areas of the basin (e.g., Hoeve & Quirt 1984; Fayek & Kyser 1997): the earliest diagenetic stage consists of hematite rims and quartz overgrowths on detrital quartz, followed by the transformation of matrix kaolinite to dickite (e.g., Beaufort *et al.* 1998; Quirt 2001), followed by partial diagenetic conversion of kaolin minerals to illite (Hoeve & Quirt 1984). Early hydrothermal alteration is represented by fine-grained illite and APS minerals (Gaboreau *et al.* 2007). Later hydrothermal alteration includes needle-shaped dravite, hematite, pyrite, and fine-grained chlorite. Post-mineralization alteration consists of fine-grained kaolinite in microfractures, partially replacing late stage hydrothermal chlorite near the unconformity (Cloutier *et al.* 2009).

Lithogeochemistry

The whole-rock geochemical data described herein is from the Cameco Corporation exploration database for the B1 trend. To reduce the influence of the high-grade mineralization on the geochemical signature of the deposit, the study database was limited to sandstone samples containing <1000 ppm U; additionally, this threshold reasonably defines the proximal edges of the deposit. This dataset includes 3608 samples (all with partial digestion analyses, 2832 of which also include total digestion). The drill holes included are distributed *c.* 21 km along the northeast to southwest B1 conductive trend (Fig. 3a). The deposit is found at the southern end of the trend, which was the focus of exploration, and therefore has a greater drill hole density (Roy *et al.* 2006).

Analytical methods

All samples were collected by Cameco from 124 drill cores between 1987 and 2014 as part of the Cree Extension project. Sandstone samples consist of composited material that comprise a number of subsample chips *c.* 1 cm in size collected approximately every 1.5 m over the 10 or 20 metre composite intervals. Whole-rock (bulk sample) geochemical analyses were performed by the Saskatchewan Research Council Geoanalytical Laboratory (SRC) using inductively coupled plasma optical emission spectrometry (ICP-OES) and inductively coupled plasma mass spectrometry (ICP-MS) techniques for major and trace element analysis. Samples were dried, and then jaw crushed to 60% at -2 mm. Subsamples of 100–200 g were obtained using a riffler and pulverized (90% at -106 µm) in a steel puck-and-ring grinder for data obtained by ICP-OES (pre-2007) or an agate ball mill (2007 and later). An agate ball mill was used for all data obtained by ICP-MS. Near-total digestion analyses utilized a mixture of ultra-pure concentrated HF:HNO_3:$HClO_4$ acids for dissolution. The resultant solutions were heated to dryness, dissolved in 5% HNO_3, and brought to volume with deionized water. Referred to herein as *total* in comparison with *partial*, total digestion does not include SiO_2 results, and As and Cr may be underrepresented. Partial digestion analyses utilized an 8:1 mixture of ultra-pure concentrated HNO_3:HCl acids for a partial dissolution of the pulps during a one hour hot water bath, followed by decanting and being brought to volume with deionized water. Major elements, Ba, Ce, Cr, La, Li, and Sr were determined with total digestion only; Hg, Sb, Se, and Te with partial digestion only; all other elements were obtained from both total and partial digestions.

In this study, both partial and total digestion data were examined as potential vectors to mineralization; partial digestion data gave more discriminating results, except for the major elements, for which only total digestion data are available. The major elements were also

examined using molar ratios to characterize the clay minerals used as vectors commonly found in and around unconformity-type U deposits (Earle & Sopuck 1989; Fayek & Kyser 1997; Zhang *et al.* 2001; Annesley & Millar 2011). The use of ratios eliminates closure issues found with compositional data and negate any differences in volume, allowing us to understand alteration transitions between endmembers as a function of proximity to mineralization (Stanley & Madeisky 1994; Davies & Whitehead 2006; Polito *et al.* 2009).

Quality assurance (QA) measures included analysis of blanks and two standards per sample batch, as well as sample replicate analysis of one replicate every 40 analyses. QA failures (deviations outside acceptable parameters) resulted in corrective action and reanalysis as required. Analytes with values less than three times the minimum detection limit for an element, per instrument, were removed from the dataset by the author to account for instrumental differences over several years of analysis and to eliminate noise related to analytical limitations (Jenner 1996).

Defining proximity to mineralization in sandstones

Seven proximity zones were established to determine the extent of the major and trace elemental distributions in the sandstones with respect to distance from the deposit (Fig. 3). These zones were defined in the horizontal dimension by varying ranges in U content and distance from the deposit location as described below. Vertically each zone extends from the unconformity to surface and is divided into stratigraphic sub-zones as per the Manitou Falls Formation lithofacies (Fig. 3d):

(1) the **Proximal Zone** is located directly above U mineralization at the unconformity (Fig. 3b) and contains sandstones with the highest U content (50–1000 ppm, partial digestion), which is a vertical corridor with a length of *c.* 350 m and depth of *c.* 550–650 m along the B1 structure;

(2) the **Main Zone** is based on the strike length of the main ore body in the basement, plus two additional areas with U >100 ppm, also in the basement (Fig. 3c), extending *c.* 1 km to the north and *c.* 0.6 km to the south of the Proximal Zone giving a total length of *c.* 2 km and a depth of *c.*550–650 m. All other zones are based on horizontal distance from this zone, with boundaries at breaks in the drill collar distribution (Fig. 3a);

(3) the **South Zone** comprises the remainder of drill holes to the south of the Main Zone, *c.* 1.5 km in length and *c.* 500–550 m in depth;

(4–7) four zones located to the north of the Main Zone, each *c.* 4.5 km in length, *c.* 600–800 m in depth, and designated **North 1 – North 4**, with North 4 being most distal.

Uranium concentrations within each proximity zone are lowest in the uppermost (MFd) lithofacies and increase toward the unconformity.

Statistical and spatial analysis

Statistical and spatial analyses of the data were examined using IBM SPSS® ver. 23 statistical software to define the lithogeochemical signature variations of the proximity zones. The background values defined in this study for major elements, and many trace elements, including U, are from Quirt (1985).

Quantile-quantile (Q-Q) plots and scatterplots were examined for each element to determine if concentrations are elevated or anomalous, and in which proximity zone these levels

occur (Fig. 4). Q-Q plots are a type of probability plot that display the ordered observed value against its calculated expected normal value; if the data is normally distributed, the results will plot along a 1:1 line. These plots are advantageous in exploration geochemistry as they display every individual data point, allowing the researcher to see how groupings of values may be significant (Grunsky 2010). Whether or not the data is distributed normally, values that are elevated and anomalous are defined visually using graphical parameters: *elevated* values are at the high end of the data distribution, whereas *anomalous* values are both elevated and discontinuous from the rest of the population, indicative of additional influences (e.g., a different geochemical process; Reimann *et al.* 2005). The *elevated* concentrations in this dataset are generally the 85th percentile and higher, with *anomalous* values generally greater than the 95th percentile; however, the specific absolute values are less relevant than determining where concentrations are elevated relative to the deposit both spatially and stratigraphically. At Millennium, this was done for each element individually, for both partial and total digestion results (Fig. 4). Results that are *elevated* or *anomalous* approaching, or within, the Proximal and Main zones without appearing in more distal areas were considered potential *pathfinder* elements and modelled in Geosoft® Target 4.5.5. for ArcGIS 3D spatial mapping software.

Results

Whole-rock lithogeochemical distributions for this dataset show that two major elements (Mg and K, Figs. 5–7); numerous trace elements (Mo, Co, Ga, Rb, Ag, Bi, Sb, Y, rare earth elements [grouped as heavy rare earth elements Dy, Er, Tb, Yb (HREE), and light rare earth elements Eu, Gd, Nd, Pr, Sm (LREE)] (Figs. 9–12); and select Pb isotope ratios (Fig. 13) exhibit quantifiable trends with proximity to elevated U.

Major elements

Plots of select major elements are shown in Figures 5–7. Major elements in the sandstones reflect the varying abundances of quartz, matrix clay minerals, and other detrital and matrix material; the latter two groups being from both detritus and diagenetic/hydrothermal fluid-rock interaction (Quirt 1985; Beaufort *et al.* 2005). Normative clay mineral abundances were calculated with major element data using a calculation optimized for the Athabasca Basin (Quirt 1995). The clay norm results (Fig. 5a) illustrate that along the entire 21 km strike of the B1 trend there are similar total clay mineral contents independent of distance from the deposit, with median values ranging from *c.* 3% in the MFd to *c.* 6% in the MFa.

When compared to background concentrations for Manitou Falls Formation sandstones, MgO and K_2O are elevated and Fe_2O_3 and Na_2O are depleted in all four lithofacies along the entire B1 trend (Quirt 1985). However, only MgO exhibits any trend with respect to the deposit location. MgO values increase with proximity to mineralization, with median values present above background within *c.* 10 km north of the deposit in the MFd, MFc, and MFa lithofacies (North 2 zone), and *c.* 6 km north of the deposit in the MFb lithofacies (North 1 zone) (Fig. 5b–c). This feature is also illustrated in the Mg/Al vs. K/Al molar element ratio diagrams (Fig. 6). These diagrams were constructed to evaluate the variations in clay mineral abundances and types, and can be used to delineate data trends between various diagenetic and alteration phases, including 'kaolin group' (dickite and kaolinite), illite, chlorite (Al-Mg-sudoite), and tourmaline (alkali-deficient dravite), all of which are associated with either sandstone diagenesis or syn- to post-hydrothermal alteration and U deposits (Tremblay 1982; Hoeve & Quirt 1984; Earle & Sopuck 1989; Zhang *et al.* 2001; among others). In Mg/Al-K/Al molar ratio space, samples that plot on the trend between the kaolin group node and the illite node are dominant >10 km from

the deposit (North 3 and North 4) and in all proximity zones within the MFb lithofacies (Fig. 6). In the MFd, MFc, and MFa lithofacies, multiple samples display a shift toward increasing Mg/Al and decreasing K/Al with proximity to mineralization. This transition from K-dominant to Mg-dominant alteration is recorded as Mg/K molar ratios >2, which are present within 6 km of the deposit in the MFd, MFc, and MFa lithofacies, and represent the 90th percentile in the Proximal zone; median Mg/K molar ratios >0.2 mark the outer, 10-km boundary in the MFd, MFc, and MFa lithofacies (Fig. 7).

Trace element haloes

For the majority of elements, the partial digestion results delineate alteration haloes and proximity to the deposit more effectively than total digestion results, particularly in the Proximal and Main zones where they can be divided into three spatial patterns: *chimney*, *hump*, and *bullseye* (Fig. 8). This terminology is descriptive in nature, determined by the visual 3D mapping results of elevated to anomalous elemental concentrations and their spatial relationship to the deposit: *chimney* refers to a vertical plume ascending to the surface directly above the central body of the deposit; *hump* refers to a wider distribution above the main and proximal zones that does not appear above the MFc lithofacies; and *bullseye* describes a lens shape with the highest concentrations in the MFb/MFa lithofacies centered above the central body of the deposit (Fig. 8 and Table 1).

The chimney-type pattern is demonstrated by Mo (Fig. 9), Co, Ga, and Rb. Elevated concentrations (partial digestion results) are vertically distributed in the Proximal and Main zones throughout all four lithofacies, forming a halo 1100–1700 m along and 400–600 m across the B1 trend (Table 1). Small localized anomalies distal from the deposit are coincident with isolated values of U >1 ppm. As concentrations increase from elevated to anomalous, the haloes

become smaller in size but remain centered over the deposit. Molybdenum and Co exhibit the most vertically extensive distributions, with anomalous values present even in the upper lithofacies (MFd).

The HREE (Dy, Er, Tb, and Yb) and Y (partial digestion) display the hump-type pattern and exhibit anomalous concentrations within the Proximal and Main zones in the MFa, MFb, and MFc lithofacies (Fig. 10). The anomalous values form rounded or conical haloes ranging from 700–1550 m along and 250–500 m across the B1 trend, mainly within 500 m but extending up to 650 m above the unconformity (Table 1). In addition to this hump above the deposit, they also have localized enrichments distally, generally corresponding to isolated zones with elevated U content, albeit at a much lower density than in the Proximal and Main zones.

The bullseye-type pattern is demonstrated by the LREE, which are elevated within the MFb lithofacies along the entire study area footprint; this was also observed by Kister *et al.* (2003) in the Shea Creek area (western Athabasca Basin). However, Eu, Gd, Nd, Pr, and Sm (partial digestion) exhibit anomalous values in the MFb and MFa lithofacies within the Proximal and Main zones, the sum of which occur as lens shapes *c.* 1150 m along and *c.* 350 m across the B1 trend (Fig. 11; Table 1). Rare isolated anomalous concentrations appear in locations distal to the deposit.

Silver, Bi, and Sb (partial digestion) also display the chimney-type to hump-type distribution patterns but are elevated almost exclusively in the Proximal or Main zone corridors; up to 650 m above the unconformity for Ag and Sb, and up to 450 m for Bi (Fig. 12; Table 1). Unlike the trace elements discussed above, these elements are either not detectable, or are at levels less than three times the instrument detection limit, for nearly all samples elsewhere in the footprint.

Lead isotope ratios

Radiogenic Pb isotopes (i.e., ^{206}Pb and ^{207}Pb) are decay products of U, and their distribution in alteration haloes can act as a geochemical vector toward U mineralization (Holk *et al.* 2003; Annesley *et al.* 2005b; Quirt 2009; Alexandre *et al.* 2012). Thresholds for Pb isotopic ratios as indicators of mineralization are defined here as: ≥35 (indicative) or ≥50 and higher (strongly indicative) for $^{206}Pb/^{204}Pb$, and ≤0.4 (indicative) or ≤0.2 (strongly indicative) for $^{207}Pb/^{206}Pb$ (Annesley *et al.* 2005b; Cloutier *et al.* 2009; Quirt 2009).

At Millennium, most samples that are indicative of mineralization are found in the Proximal and Main zones (Fig. 13). Of 81 samples with $^{206}Pb/^{204}Pb$ values ≥35, 51 are present in these zones, mainly within the MFa lithofacies as a contiguous halo up to 65 metres from the unconformity. Twenty samples occur in the North 4 zone. Although most of these samples are not enriched in U, elevated U is present in other samples from the same drill holes. Twenty-six samples with $^{207}Pb/^{206}Pb$ values of 0.4 to 0.2 are present in the Proximal zone, mirroring the $^{206}Pb/^{204}Pb$ ≥35 locations, although with a smaller halo. Only eight other occurrences are noted, in North 2 MFa and North 4 MFa, MFc, and MFd; six of these eight are associated with elevated U contents.

Discussion

The Millennium deposit is predominantly basement-hosted, with over three-quarters of the resource situated 100–150 m below the sub-Athabasca unconformity (650–700 m depth) (Fig. 2b–c). Throughout the Millennium study area there are distinctive geochemical and mineralogical patterns in the Manitou Falls Formation sandstones, ranging from several kilometres distal to within tens of metres of mineralization. This host-rock alteration may

represent a compositional and mineralogical record of the same fluid-rock interaction processes that formed U mineralization (Hoeve & Quirt 1984; Cuney 2005; Kerr & Wallis 2014). These processes are demonstrated by increased concentrations of major and trace elements, forming alteration haloes along the strike of the B1 trend, in varying dimensions. This geochemical footprint is constrained by drill hole distribution across strike and to the south of the deposit, and the full extent of the haloes in those directions are therefore unknown; however, the deposit location is highlighted where these haloes coincide.

Geochemical halo patterns

Total clay mineral abundances are related to lithostratigraphy and increase with stratigraphic depth, as demonstrated by the clay mineral norm results throughout the 21-km footprint of the B1 trend (Fig. 5a). Total abundances do not display any trend toward mineralization, suggesting that the original clay minerals in each stratigraphic unit were altered without a significant net gain or loss in the total amount of clay minerals in each lithostratigraphic volume. However, K_2O and MgO are present in levels above background, which demonstrate the presence of hydrothermal alteration from fluids enriched in both K and Mg. At Millennium, Cloutier *et al.* (2009) suggested that K was derived from basinal brines, and that the majority of the Mg was sourced from the basement; the enrichment of both elements in the sandstones (Fig. 5b–c) implies that the basinal brines responsible for deposit formation had first entered, reacted with, and then exited the basement. This is consistent with the paragenetic sequence described by Cloutier *et al.* (2009) where illite (K-alteration) comprised the early stages of alteration, and dravite and chlorite (Mg-alteration) the later stages. The distal edge of the Mg-alteration envelope is defined by median MgO values greater than background, which first appear approximately 10 km north of the deposit in the MFd, MFc, and MFa lithofacies;

MgO concentrations increase with proximity and are highest within 2 km of the deposit location (Fig.5b–c).

The Millennium deposit sits within and near semi-regional illite, dravite, and chlorite sandstone anomalies (Fig. 1b; Earle & Sopuck 1989). To better visualize the relationship between K_2O (illite) and MgO (dravite, chlorite) on a district scale, and how their concentrations change with respect to distance to mineralization, molar element ratios (Mg/Al vs. K/Al) were utilized (Fig. 6; Stanley & Madeisky 1994; Davies & Whitehead 2006). Because total clay abundances are roughly similar across the study area for a given stratigraphic unit, and all three minerals are found in variable amounts in all locations, the molar element ratios better demonstrate the transitions or mixtures between these endmembers in spatial association with the deposit, therefore having vectoring potential. The distal zones North 3 and North 4, which are 10–20 km north of the deposit, contain samples that plot from the kaolin group (dickite ± kaolinite) node to the illite node almost exclusively (Fig. 6). The Al-dominant samples can be either diagenetic (i.e., background), or a consequence of late fracture infilling (Earle & Sopuck 1989; Beaufort *et al.* 1998; Cloutier *et al.* 2009). The K-dominant samples with minor Mg are either diagenetic illite alteration or early hydrothermal illite alteration (Hoeve & Quirt 1984; Cloutier *et al.* 2009). All samples within the MFb lithofacies, irrespective of proximity to mineralization, plot on this trend between these two nodes and are weighted toward the Al-dominant mineral. This Al-dominance is likely representative of dickite, as Roy *et al.* (2006) described the 'middle' lithofacies as dickite-dominated. In contrast, proximity zones within 10 km of the deposit in the MFa, MFc, and MFd lithofacies all contain samples that plot on a trend between the illite and Mg-rich alkali-deficient dravite and sudoite nodes, with those closest to the latter endmembers within 1 km of the deposit. This geochemical trend is interpreted as later-

stage hydrothermal alteration that includes replacement or overprinting of kaolin and illite by alkali-deficient dravite and sudoite via Mg- and B-bearing fluids, originally of basinal origin but highly altered by fluid-rock interaction in the basement (e.g., Earle & Sopuck 1989; Cloutier *et al.* 2009).

To quantify the sample transitions between the illite, sudoite, and alkali-deficient nodes seen in the molar element ratio diagram (i.e., K-dominant to Mg-dominant), the molar ratios of Mg/K were examined. The Mg/K median values in North 3 and North 4 are <0.2 and increase significantly (1.5–2x) inside the 10-km envelope; individual values >2 increase with proximity to the deposit, marking the 6-km envelope in the MFd, MFc, and MFa lithofacies (Fig. 7). The MFb has a muted overall trend but contains anomalous Mg/K values >0.6 that mark the 6-km envelope as well. This muted signature suggests that original structural or permeability differences may have impeded fluid-rock interaction and alteration of the MFb in comparison to the other lithofacies. The proximal signature characterized by the Mg/K values is suggestive of greater concentrations of sudoite and alkali-deficient dravite in the Proximal and Main zones. The relative increase in Mg/K may reflect the overprinting of earlier illite by the Mg-dominant minerals (e.g., Percival & Kodama 1989), as Al-Mg-sudoite ± alkali-deficient dravite are paragenetically later (Cloutier *et al.* 2009). The largest Mg/K differential is present directly above the deposit and within a 1–2 km strike along the B1 trend, and is indicative of enhanced fluid-rock interaction, which is potentially related to the greater number of faults and fractures proximal to mineralization. Mg-enriched fluids likely re-entered the basin along these faults and fractures, a common location for both sudoite and alkali-deficient dravite as indicators for unconformity-type U deposits (e.g., Hoeve & Quirt 1984; Fayek & Kyser 1997).

Whereas the major elements display larger haloes representative of host-rock alteration and clay mineral distributions (Hoeve & Quirt 1984), several trace elements form distinct patterns (i.e. chimney, hump, and bullseye patterns; Fig. 8) of elevated to anomalous concentrations within, or increasing toward, the Proximal or Main zones. This is particularly clear with partial digestion results, which provide a better mapping of the fluid flow pathways associated with mineralization because the method does not completely digest refractory heavy minerals (Jackson 2010). The chimney patterns exhibited by Mo, Co, Rb, and Ga are distributed vertically from the unconformity to surface directly above the deposit and are interpreted to reflect element transport upwards from the basement along faults or fractures (Fig. 9), either during the ore forming event or through subsequent secondary dispersion events. These elements are either redox-sensitive pathfinder elements (e.g., Mo, Co) or coincident with clay alteration in the sandstones and substitution for major elements in clay minerals (e.g., Ga for Al; Rb for K).

The hump-type pattern is transitional from the vertical chimneys to a conical shape above Millennium. Elevated HREE (Fig. 10), Y, and $^{206}Pb/^{204}Pb$ and $^{207}Pb/^{206}Pb$ ratios are more restricted than chimney elements; they are concentrated in the middle to lower lithofacies (MFc–MFa), up to 500 m above the unconformity. Anomalous concentrations rarely extend above the MFc and, in the case of the Pb isotopes, are mainly restricted to the MFa (Fig. 13). This type of pattern is interpreted to reflect HREE-Y-U incorporation into alteration-related xenotime and uraninite associated with deposit formation, and subsequent *in situ* U decay to ^{206}Pb and ^{207}Pb (Quirt *et al.* 1991; Fayek & Kyser 1997; Holk *et al.* 2003).

The bullseye-type pattern is recorded by LREE, which are predominantly stratiform in distribution and concentrated in the MFb-MFa lithofacies throughout the entire study area, with little discernible relationship to deposit location. However, anomalous values of some LREE

(Eu, Gd, Nd, Pr, Sm) are present within the Proximal and Main zones above the deposit, with small haloes horizontally distributed within the MFb and MFa, up to 450 m above the unconformity and 600 m along the B1 trend (Fig. 11, Table 1). Detrital heavy minerals are more prevalent in the MFb lithofacies (Roy *et al.* 2006), and likely account for the stratiform distribution of LREE in total, whereas the anomalous LREE in the bullseye haloes are likely related to hydrothermal alteration APS minerals (Gaboreau *et al.* 2005, 2007).

In addition to the above trace element patterns, there are enrichments in Ag, Bi, and Sb in the Proximal or Main Zones in all lithofacies (Fig. 12). Approximately 90% of all samples with confidently measurable concentrations of these elements are located here and are below detection limits elsewhere in the study area. This suggests their enrichments were due to increased fluid-rock interaction, qualifying these elements as indicators of the greatest amounts of hydrothermal activity.

Implications for exploration

Anomalous U is present in the Manitou Falls Formation sandstones overlying the Millennium deposit and up to 20 km distal (Fig. 3b); for exploration purposes, it is beneficial to understand which of these showings are spatially related to the majority of the deposit located below the unconformity. The alteration haloes described above, which extend several kilometres north of the deposit, provide a weak but identifiable geochemical footprint that differentiates the areas hosting distal U from proximal U, and the elevated to anomalous concentrations of select elements within these haloes highlight the location of the mineralization at depth. These hydrothermal haloes likely extend further to the south of the deposit as well; however, delineating their borders in this area is difficult due to a lack of drill holes.

There are two main distributions of elemental and mineralogical pathfinders within this footprint: (1) larger-scale haloes 6–10 km north along strike of the deposit, along the B1 trend, involving the major elements K and Mg and related normative clay mineralogy; and (2) smaller haloes of several trace elements positioned directly above the deposit that extend *c.* 0.6–1.5 km along the B1 trend. These haloes are present in all lithofacies, up to 600 m above the unconformity, and their nesting is key to exploration. The small, isolated areas of anomalously high U (2–5 ppm) in the distal zone North 4 (Fig. 3b) do not coincide with either of these haloes, suggesting that a potential exploration area should exhibit evidence of alteration and potential mineralization processes in addition to U itself (Figs 14–15). The first-order, larger-scale haloes are representative of the shift from K-dominant to Mg-dominant mineral species, with median Mg/K values above background appearing up to 10 km north of the deposit (Fig. 7), along with rare, anomalously high U (2–5 ppm). Within this area lie the second-order alteration haloes, along with most of the anomalous U (2–5 ppm). These haloes are not as extensive but are still 2–5 times greater in scale than the greatest concentrations of U (50–1000 ppm) seen at the unconformity, directly above the deposit (Table 1). These haloes reflect clay mineral formation (Ga, Rb substitution in clay minerals) and other elements associated with mineralization through redox-related and other processes (Mo, Co, U, HREE, LREE, radiogenic Pb). At Millennium, the combination of molar element ratios and trace element distribution patterns are representative of host-rock clay mineral alteration, and the results herein—specifically where these haloes coincide—illustrate scalable vectors to mineralization that record and characterize the mineralizing processes related to unconformity-type U formation.

Conclusions

The Millennium deposit is an unconformity-type U deposit with the majority of mineralization located greater than 650 m below the surface, *c.* 150 m below the unconformity, but with lenses extending to the unconformity itself. Despite these depths and the simple-type mineralization (monomineralic pitchblende), a unique geochemical signature is present in the Manitou Falls Formation sandstones that extends hundreds of metres vertically and horizontally from the deposit that may reflect ore forming processes and associated fluid-rock interaction. Molar element ratios of Mg and K to Al exhibit significant changes within 10 km of the deposit, notably within the upper lithofacies, that signify hydrothermal host-rock alteration consistent with the formation of chlorite (Al-Mg-sudoite) and alkali-deficient dravite, minerals known to be associated with unconformity-type U deposits. Along the B1 conductive trend the molar ratios Mg/K increase with proximity to the deposit. Within 1.5 km of the deposit, several trace elements, including U, REE, and Y, form haloes of elevated to anomalous concentrations that intensify with proximity to the unconformity and the deposit location. These geochemical distributions likely signify primary dispersion along fluid pathways involved in the mineralizing system, in particular, Mo, Co, Rb, and Ga, which form haloes shaped as a vertical plume extending from the unconformity to upper lithofacies. This suggests that vectoring toward a deep, monomineralic U deposit is possible using whole-rock geochemistry from overlying sandstones.

ACKNOWLEDGEMENTS

Many thanks to Cameco Corp. for providing the data and multiple illuminating discussions. Astute additional editing by Michael Buschette, Jonathan Cloutier, and Stefanie Lode was essential to the clarity of this paper, which is NSERC-CMIC Mineral Exploration Footprints Project Contribution Number 108. We thank GEEA reviewers Paul Alexandre and Irvine

Annesley, and editor Gwendy Hall, for their comments and suggestions which greatly contributed to its improvement.

FUNDING INFORMATION

Funding was provided by the Natural Sciences and Engineering Research Council of Canada and the Canada Mining Innovation Council Footprints Project, which involved funding from industry partners and funding from the NSERC Collaborative Research and Development Program. Logistical support was generously provided by Cameco Corp. Additional funding was provided by the NSERC-Altius Industrial Research Chair to Piercey, funded by NSERC, Altius Resources Inc., and the Research and Development Corporation of Newfoundland and Labrador, and an NSERC Discovery Grant to Piercey.

FIGURE CAPTIONS

Fig. 1: (**A**) Simplified geological map of the Athabasca Basin and underlying Precambrian domains in northern Saskatchewan and Alberta. The Snowbird Tectonic Zone is the boundary between the Rae and Hearne provinces; the later Trans-Hudson orogen was responsible for the accretion of the Reindeer Zone to the eastern Hearne. A large number of unconformity-type U deposits are found in the eastern basin. Adapted from Card *et al.* (2007), and Cloutier *et al.* (2009). (**B**) Geological relationships in the southeastern Athabasca Basin, showing the location of selected uranium deposits relative to the Wollaston-Mudjatik Transition Zone (WMTZ), and regional zones of alteration. Adapted from Earle & Sopuck (1989), Jefferson *et al.* (2007), and Jeanneret *et al.* (2016).

Fig. 2: Millennium deposit geology of the basement, looking north. Depths are in metres above sea level (ASL); sandstones in the vicinity of the deposit extend to approximately 500 m ASL. (**A**) Cross section at the Millennium deposit discovery hole (CX-040) and surrounding drill holes. The Mother fault is a major structure in the basement rocks of the Millennium deposit. Mineralization is associated with a reverse fault that cross cuts the graphitic Marker Unit in the basement above the Mother fault. Although a majority of the mineralization is located in the basement rocks, up to 20% can be found at the unconformity. Adapted from Cameco internal memo, J. Mukwakwami (2013). (**B**) Simplified alteration and mineralization of the basement rocks, looking north, adapted from Roy *et al.* (2006) and Cloutier *et al.* (2009). Three alteration zones are described: distal saussurite-sericite alteration found furthest from mineralization in basement rocks above and below the Mother fault, a central illite-dravite halo that is associated with and crosscut by the Mother fault, and a proximal chlorite-illite-halo associated with mineralization. Hematite, chlorite, and a graphitic marker unit associated with the upper reverse fault are also found in proximity to mineralization. (**C**) Cross section showing depth of unconformity and deposit in relation to overlying Manitou Falls Formation, the focus of analysis. Adapted from Roy *et al.* (2006).

Fig. 3: The Millennium deposit study area. (**A**) Plan view of the study area. Black dots are drill hole collars. Coordinates are WGS 84 UTM 13N; star is deposit location. (**B**) Longitudinal section along the B1 trend; view of the sandstones with U >1 ppm (partial digestion), looking

due east. Vertical lines are drill hole traces. (**C**) As in (**B**) of the basement with U >100 ppm (partial digestion). (**D**) Proximity zones based on the location of U in the sandstones (Prox-A,-B,-C,-D) and basement (Main A,B,C,D on either side). Not to scale. Each lithofacies is considered separately in the quantification of elevated or anomalous results.

Fig. 4: Simplified example of how data were examined in this study. (**A**) Footprint was divided into proximity zones determined by horizontal distance of drill collar from deposit location, marked with a star (P, proximal). (**B**) All data from a single element was plotted with a quantile-quantile (Q-Q) plot. Breaks in data distinguish anomalous (red circles) from elevated (blue circles) results. (**C**) Results plotted with regard to proximity zone. If the elevated to anomalous values were found to change with proximity to the deposit location, they were mapped in 3D. (**D**) Plan view of drill holes containing elevated (blue) to anomalous (red) values, showing a spatial relationship to the deposit location.

Fig. 5: Box-and-whisker plots illustrating total clay mineral and MgO content across study area. Each box is the interquartile range (IQ) which represents the 25^{th}–75^{th} percentile; the dark line within the box notes the 50^{th}. The whisker dimension covers 1.5 times the IQ range. The dots represent values 1.5–3 times the IQ range, and the stars greater than 3 times the IQ range. **A**) The total amount of clay minerals present estimated from a clay norm calculation. The two lower lithofacies (MFb–MFa) contain median values of 6%, the MFc median values of 4%, and the MFd (uppermost) 2.5%. Values are generally consistent across the 20-km study area. (**B**) MgO concentration in the upper two Manitou Falls Formation lithofacies as compared to background values of Quirt (1985): 0.03 ± 0.005%, marked on plot with horizontal lines. Concentrations increase with proximity to the deposit (to the right of the plot, deposit location marked with star). (**C**) MgO concentration in the lower two lithofacies. Background values are 0.03 ± 0.01%, marked on plot with horizontal lines. As in the upper two lithofacies, concentrations increase with proximity to the deposit. All results are from total digestion, ICP-OES; n = 2831. N4 = 228, N3 = 209, N2 = 361, N1 = 417, Main = 581, P = 886, S = 149. The star marks the deposit location in all plots.

Fig. 6: Molar element ratio plots demonstrate the varying contents of Mg and K in relation to the deposit location, representative of Al-Mg-sudoite and alkali-deficient dravite alteration. In the least-altered locations, greater than 10 km from the deposit (North 4 and North 3), samples plot on the trend between the kaolin group and illite nodes almost exclusively. Within 10 km of the deposit (North 2), samples shift toward the alkali-deficient dravite and sudoite nodes in the MFd, MFc, and MFa lithofacies. This shift intensifies with proximity to the deposit in all lithofacies but the MFb. Sudoite and illite formulas are from Cloutier *et al.* (2009); alkali-deficient dravite formula estimated from Garofalo *et al.* (2000) and Zhang *et al.* (2001). Total number of samples = 2775. Samples per proximity zone: N4 = 228, N3 = 209, N2 = 361, N1 = 361, Main = 581, Proximal = 886, South = 149.

Fig. 7: The molar ratios of Mg/K increase with proximity to the deposit (to the right of each plot; deposit location marked with star). Box-and-whisker symbols represent data ranges as noted in Figure 5. Median values of MFd, MFc, and MFa lithofacies inside the 10 km halo (solid gray vertical boundary) are >0.2 (solid horizontal line). MFb exhibits values >0.37 (solid horizontal

line, 95th percentile for MFb). The following values are present within the 6 km halo: MFd >2.0, MFc >1.0, MFb >0.55 (horizontal dotted lines). MFa shows significant increases with median values >1.0 (dash-dot line) above deposit location.

Fig. 8: Elevated and anomalous concentrations of select elements fit into three broad categories of spatial distribution in relation to the main mineralized body. For all three, halo dimensions diminish as concentration increases. (**A**) The 'chimney' elements (Mo, Co, Ga, Rb, partial digestion) appear as vertical plumes directly above the basement deposit, with Mo and Co ascending to the shallowest lithofacies (MFd). Isolated elevated concentrations are also seen distal from the deposit. (**B**) The 'hump' elements (HREE, Y; partial digestion) form a more rounded shape which in lesser concentrations does not ascend to the MFd. The halo is centered over the deposit and is non-contiguous. As with the chimney group, there are distal, isolated elevated values, mainly within the MFa. (**C**) The 'bullseye' elements (LREE; partial digestion) are concentrated within the lower sandstone (MFb) and appear stratiform throughout the footprint; however, above the deposit body anomalous values are apparent.

Fig. 9: Molybdenum (partial digestion) is shown here as an example of the process used to determine spatial relationships of elevated and anomalous concentrations to the deposit location, noted by the star. (**A**) The 3D maps show the "chimney" pattern evident at the 87th percentile (≥0.5 ppm) of concentrations grouped above the deposit location and present to the surface in a vertical distribution. The halo becomes less contiguous as the concentrations increase but remains within the Proximal and Main zones. Vertical lines are drill hole traces. (**B**) Quantile-quantile plots show the data distribution within each lithofacies. Dotted (0.5 ppm) and solid (1.5 ppm) lines represent the cut-off for the upper and lower 3D maps above. The first break in data indicative of anomalies or distinct populations occurs between 0.5–0.6 ppm, with the truly anomalous data >2 ppm in all lithofacies. (**C**) Scatter plots demarcated by proximity show the anomalous data that appear in the North 1 (N1) zone in lithofacies MFa–MFc, which appear in red in the 3D maps. Dotted and solid lines are equivalent to those in (**A**) and (**B**).

Fig. 10: The sum of all HREE (partial digestion) is shown as an example of the process used to determine spatial relationships of elevated and anomalous concentrations to the deposit location, noted by the star. (**A**) The 3D maps show the 'hump' pattern evident at the 87th percentile (≥ 0.5 ppm) of concentrations grouped above the deposit location as well as areas distal. The halo becomes less contiguous as the concentrations increase but remains within the Proximal and Main zones. Vertical lines are drill hole traces. (**B**) Quantile-quantile plots show the data distribution within each lithofacies. Dotted and solid black lines shown are at 0.5 and 0.7 ppm, which represent the cut-off for the lower and upper 3D maps above. (**C**) The scatter plots demarcated by proximity show the anomalous data that appear in the North 1 and North 2 (N1, N2) zones in lithofacies MFa–MFb which appear in red in the 3D maps. Dotted and solid lines are equivalent to those in (**A**) and (**B**).

Fig. 11: The sum of all LREE (partial digestion) is shown as an example of the process used to determine spatial relationships of elevated and anomalous concentrations to the deposit location, noted by the star. (**A**) The 3D maps show the 'bullseye' pattern evident at the 78th percentile (≥ 5 ppm) of concentrations grouped above the deposit location as well as areas distal. The halo becomes less contiguous as the concentrations increase but remains within the Proximal and Main zones. Vertical lines are drill hole traces. (**B**) Quantile-quantile plots show the data

distribution within each lithofacies. Dotted and solid black lines shown are at 5 and 8 ppm, which represent the cut-off for the lower and upper 3D maps above. (**C**) The scatter plots demarcated by proximity show the majority of data are located within the MFb. Dotted and solid lines are equivalent to those in (**A**) and (**B**).

Fig. 12: Silver, Bi, and Sb concentrations are either below analytical detection limit or less than three times the instrument detection limit (0.03 ppm) throughout most of the footprint, with *c.* 90% of the confidently measurable concentrations present in the Proximal and Main zones; these are the values shown above the solid horizontal line. The implication is that the Proximal and Main zones underwent a greater degree of fluid-rock interaction than the other areas; these elements are therefore an indicator of a location in the footprint of increased activity and possible mineralization.

Fig. 13: Lead isotope results (partial digestion) in the sandstones above the Millennium deposit, separated by lithofacies with regard to proximity to deposit (located with P, star). (**A**) $^{206}Pb/^{204}Pb$ values. Ratios indicative of mineralization are present mainly within the Proximal Zone and in the MFa of the Main Zone. Anomalously indicative ratios in North 4 are located in drill holes with samples containing U >1 ppm. (**B**) As in (**A**), but with $^{207}Pb/^{206}Pb$ values. Sample analyses (n) for each proximity zone: North 4 = 194, North 3 = 102, North 2 = 255, North 1 = 265, Main = 558, Proximal = 762, South = 122.

Fig. 14: Plan view of study footprint, with vectors as defined through whole rock geochemistry. The median values of Mg/K (molar) demonstrate the 10-km envelope as they increase 1.5–2x within these areas, and with proximity to the deposit. Trace elements, including U, are shown highlighting the Main and Proximal corridors through all four lithofacies, which is a 1.9-km strike above the deposit location. Anomalously high values of U, rare and isolated, are found in the north of the study area but are not associated with any deposit. This map demonstrates the validity of utilizing the major and trace element haloes as a vectoring device, which overlap at the location of the deposit (Main, Proximal). Because the area to the south of the deposit is limited by drill hole distribution, it is not fully defined geochemically and the halo boundaries are therefore left open.

Fig. 15: Stylized longitudinal section view of study footprint, as in Fig. 14, with vectors as defined through whole rock geochemistry. Not to scale. The median values of Mg/K (molar) demonstrate the 10-km envelope as they increase 1.5–2x within these areas, and with proximity to the deposit. The 6-km envelope is defined through anomalous Mg/K molar ratios >2 in the MFd, MFc, and MFa lithofacies. Elevated concentrations of trace elements are vertically distributed within the Main and Proximal corridors, which is a 1.9 km strike above the deposit location.

Table 1: Halo dimensions of those elements found with a spatial relationship to the Millennium deposit location. Measurements were taken in Target relative to the strike of the B1 trend; 'along strike' is parallel to the trend (NE-SW), 'across strike' is perpendicular (NW-SE). Halo dimensions across strike are constrained by hole locations and largest measurements may not be representative of true size. The highest concentrations of U present in the sandstones directly above the deposit (50 – 1000 ppm, partial digestion) provide a halo with which the vector

elements are compared. Measurements of these vector haloes are conservative estimates to nearest 50 m from 3D projections of 25-m cells with an inverse distance weighted algorithm. Not all patterns are contiguous.

REFERENCES

Alexandre, P., Kyser, K., Jiricka, D., & Witt, G. (2012). Formation and evolution of the Centennial unconformity-related uranium deposit in the South-Central Athabasca Basin, Canada. *Economic Geology*, *107*(3), 385–400. http://doi.org/10.2113/econgeo.107.3.385

Alexandre, P., Kyser, K., Polito, P., & Thomas, D. (2005). Alteration mineralogy and stable isotope geochemistry of Paleoproterozoic basement-hosted unconformity-type uranium deposits in the Athabasca Basin, Canada. *Economic Geology*, *100*(8), 1547–1563. http://doi.org/10.2113/gsecongeo.100.8.1547

Alexandre, P., Kyser, K., Thomas, D., Polito, P., & Marlat, J. (2009). Geochronology of unconformity-related uranium deposits in the Athabasca Basin, Saskatchewan, Canada and their integration in the evolution of the basin. *Mineralium Deposita*, *44*(1), 41–59. http://doi.org/10.1007/s00126-007-0153-3

Annesley, I. R., & Millar, R. (2011). Tourmaline-and sulfide-bearing graphitic pelitic gneisses of the Paleoproterozoic Wollaston Group, northern Saskatchewan: new insights into understanding the carbon-sulfur-boron-uranium geochemical system with implications for U/C-type uranium deposits. In *25th International Applied Geochemistry (IAGS) Symposium, Finland*, 111.

Annesley, I. R., Madore, C., & Hajnal, Z. (2003). Wollaston–Mudjatik transition zone: its characteristics and influence on the genesis of unconformity-type uranium deposits. *In* Cuney, M. (ed.), *Proceedings of the International Conference on Uranium Geochemistry: Nancy, France*, p. 55–58.

Annesley, I. R., Madore, C., & Portella, P. (2005a). Geology and thermotectonic evolution of the western margin of the Trans-Hudson Orogen: evidence from the eastern sub-Athabasca basement, Saskatchewan. *Canadian Journal of Earth Sciences*, *42*(4), 573–597. http://doi.org/10.1139/e05-034

Annesley, I. R., Mercadier, J., Verran, D., & Pascal, M. (2017). U-Pb isotopic ages and associated REE geochemistry from the Phoenix and Gryphon uranium deposits (Wheeler River), Athabasca Basin, Saskatchewan, Canada. In *Proceedings of the 14th Biennial SGA Meeting, Mineral Resources to Discover*, Quebec, (2), 707–710.

Annesley, I. R., McCready, A. J., Madore, C., Kamo, S. L., & Kwok, K. K. (2007). U-Pb age of overthrusting and reactivation at Cree Extension: structural preparation to the Millennium

U deposit, Saskatchewan. In *Proceedings of the 9th Biennial SGA Meeting, Digging Deeper*, Dublin, Ireland (2), 1209–1212.

Annesley, I. R., Holston, A., McCready, A. J., Kusmirski, R., Billard, D., & Hochstein, R. (2005b). Lead isotopes from Moore Lakes, Saskatchewan: New insights into palaeofluid flow in the Athabasca Basin In *Uranium production and raw materials for the nuclear fuel cycle-Supply and demand, economics, the environment and energy security: International Atomic Energy Agency Proceedings Series* (IAEA-CN-128*)*, 48–51.

Ansdell, K. M. (2005). Tectonic evolution of the Manitoba-Saskatchewan segment of the Paleoproterozoic Trans-Hudson Orogen, Canada. *Canadian Journal of Earth Sciences*, *42*(4), 741–759. http://doi.org/10.1139/e05-035

Armstrong, R. L., & Ramaekers, P. (1985). Sr isotopic study of Helikian sediment and diabase dikes in the Athabasca Basin, northern Saskatchewan. *Canadian Journal of Earth Sciences*, *22*(3), 399–407.

Beaufort, D., Patrier, P., Laverret, E., Bruneton, P., & Mondy, J. (2005). Clay alteration associated with Proterozoic unconformity-type uranium deposits in the East Alligator Rivers uranium field, Northern Territory, Australia. *Economic Geology*, *100*(3), 515–536. http://doi.org/10.2113/gsecongeo.100.3.515

Beaufort, D., Cassagnabere, A., Petit, S., Lanson, B., Berger, G., Lacharpagne, J. C., & Johansen, H. (1998). Kaolinite-to-dickite reaction in sandstone reservoirs. *Clay Minerals*, *33*(2), 297–316.

Cameco Corporation (2015). *Reserves & Resources - Millennium - Uranium Projects - Businesses - Cameco*. *Cameco.com*. Retrieved 19 September 2016, from https://www.cameco.com/businesses/ uranium-projects/millennium/reserves-resources.

Card, C. D., Pană, D., Portella, P., Thomas, D. J., & Annesley, I. R. (2007). Basement rocks to the Athabasca basin, Saskatchewan and Alberta. *In* Jefferson C.W. & Delaney, G. (eds.), *EXTECH IV: Geology and Uranium EXploration TECHnology of the Proterozoic Athabasca Basin, Saskatchewan and Alberta*: Geological Survey of Canada, Bulletin 588, 69–87.

Card, C. D., Bethune, K. M., Rayner, N., & Creaser, R. A. (2018). Characterising the southern part of the Hearne Province: A forgotten part of Canada's shield revisited. *Precambrian Research*, *307*, 51–65. https://doi.org/10.1016/j.precamres.2018.01.002

Chi, G., Bosman, S., & Card, C. (2013). Numerical modeling of fluid pressure regime in the Athabasca basin and implications for fluid flow models related to the unconformity-type uranium mineralization. *Journal of Geochemical Exploration*, *125*, 8–19. http://doi.org/10.1016/j.gexplo.2012.10.017

Cloutier, J., Kyser, K., Olivo, G. R., Alexandre, P., & Halaburda, J. (2009). The Millennium uranium deposit, Athabasca Basin, Saskatchewan, Canada: an atypical basement-hosted unconformity-related uranium deposit. *Economic Geology*, *104*(6), 815–840. http://doi.org/10.2113/gsecongeo.104.6.815

Corrigan, D., Pehrsson, S., Wodicka, N., & de Kemp, E. (2009). The Palaeoproterozoic Trans-Hudson Orogen: a prototype of modern accretionary processes. *Geological Society, London, Special Publications*, *327*(1), 457–479. http://doi.org/10.1144/SP327.19

Creaser, R. A., & Stasiuk, L. D. (2007). Depositional age of the Douglas Formation, northern Saskatchewan, determined by Re-Os geochronology. *In* Jefferson C.W. & Delaney, G. (eds.), *EXTECH IV: Geology and Uranium EXploration TECHnology of the Proterozoic Athabasca Basin, Saskatchewan and Alberta*: Geological Survey of Canada, Bulletin 588, 341–345.

Cui, T., Yang, J., & Samson, I. M. (2012). Tectonic deformation and fluid flow: implications for the formation of unconformity-related uranium deposits. *Economic Geology*, *107*(1), 147–163. http://doi.org/10.2113/econgeo.107.1.147

Cuney, M. L. (2005). World-class unconformity-related uranium deposits: key factors for their genesis. *In* Mao, J., Bierlein, F. P. (eds.), *Mineral Deposit Research: Meeting the Global Challenge* (pp. 245–248). Springer Berlin Heidelberg. http://doi.org/10.1007/3-540-27946-6_64

Cuney, M. (2009). The extreme diversity of uranium deposits. *Mineralium Deposita*, *44*(1), 3–9. http://doi.org/10.1007/s00126-008-0223-1

Dargent, M., Truche, L., Dubessy, J., Bessaque, G., & Marmier, H. (2015). Reduction kinetics of aqueous U (VI) in acidic chloride brines to uraninite by methane, hydrogen, or C-graphite under hydrothermal conditions: Implications for the genesis of unconformity-related uranium ore deposits. *Geochemica et Cosmochimica Acta*, *167*, 11–26. http://doi.org/10.1016/j.gca.2015.06.027

Davies, J. F., & Whitehead, R. E. (2006). Alkali-alumina and MgO-alumina molar ratios of altered and unaltered rhyolites. *Exploration and Mining Geology*, *15*(1-2), 75–88. http://doi.org/10.2113/gsemg.15.1-2.75

Earle, S. A. M., & Sopuck, V. J. (1989). Regional lithogeochemistry of the eastern part of the Athabasca Basin uranium province, Saskatchewan, Canada. *In* Muller-Kahle, E., (ed.), *Uranium resources and geology of North America: International Atomic Energy Agency,* TECDOC-500, 263–296.

Fayek, M. & Kyser, T. (1997). Characterization of multiple fluid-flow events and rare-earth-element mobility associated with formation of unconformity-type uranium deposits in the Athabasca Basin, Saskatchewan. *The Canadian Mineralogist, 35,* 627–658.

Fayek, M., Camacho, A., Beshears, C., Jiricka, D., & Halaburda, J. (2010). Two Sources of Uranium at the Millennium Uranium Deposit, Athabasca Basin, Saskatchewan, Canada. In *Geological Association of Canada—Mineralogical Association of Canada 2010 (Calgary) Annual Conference Abstracts Volume,* 4 p.

Gaboreau, S., Beaufort, D., Vieillard, P., Patrier, P., & Bruneton, P. (2005). Aluminum phosphate–sulfate minerals associated with Proterozoic unconformity-type uranium deposits in the East Alligator River Uranium Field, Northern Territories, Australia. *The Canadian Mineralogist*, *43*(2), 813–827. http://doi.org/10.2113/gscanmin.43.2.813

Gaboreau, S., Cuney, M., Quirt, D., Beaufort, D., Patrier, P., & Mathieu, R. (2007). Significance of aluminum phosphate-sulfate minerals associated with U unconformity-type deposits: The Athabasca basin, Canada. *American Mineralogist*, *92*(2-3), 267–280. http://doi.org/10.2138/am.2007.2277

Garofalo, P., Audétat, A., Günther, D., Heinrich, C. A., & Ridley, J. (2000). Estimation and testing of standard molar thermodynamic properties of tourmaline end-members using data of natural samples. *American Mineralogist*, *85*(1), 78–88.

Grunsky, E. C. (2010). The interpretation of geochemical survey data. *Geochemistry: Exploration, Environment, Analysis*, *10*, 27–74. http://doi.org/10.1144/1467-7873/09-210

Hecht, L., & Cuney, M. (2000). Hydrothermal alteration of monazite in the Precambrian crystalline basement of the Athabasca Basin (Saskatchewan, Canada): implications for the formation of unconformity-related uranium deposits. *Mineralium Deposita*, *35*(8), 791–795. http://doi.org/10.1007/s001260050280

Hiatt, E. E., & Kyser, T. K. (2007). Sequence stratigraphy, hydrostratigraphy, and mineralizing fluid flow in the Proterozoic Manitou Falls Formation, eastern Athabasca Basin, Saskatchewan. *In* Jefferson C.W. & Delaney, G. (eds.), *EXTECH IV: Geology and Uranium EXploration TECHnology of the Proterozoic Athabasca Basin, Saskatchewan and Alberta:* Geological Survey of Canada, Bulletin 588, 489–506.

Hoeve, J., & Quirt, D. H. (1984). Mineralization and host rock alteration in relation to clay mineral diagenesis and evolution of the Middle-Proterozoic, Athabasca Basin, northern Saskatchewan, Canada. Saskatchewan Research Council, SRC Technical Report 187, 202 p.

Hoeve, J., & Sibbald, T. I. (1978). On the genesis of Rabbit Lake and other unconformity-type uranium deposits in northern Saskatchewan, Canada. *Economic Geology*, *73*, 1450–1473.

Hoeve, J., Rawsthorn, K., & Quirt, D. (1981). Uranium metallogenetic studies: clay mineral stratigraphy and diagenesis in the Athabasca Group. *In* Summary of Investigations 1981, Saskatchewan Geological Survey, Miscellaneous Report 81-4, p. 76–89.

Hoffman, P. F. (1988). United Plates of America, the birth of a craton: Early Proterozoic assembly and growth of Laurentia. *Annual Review of Earth and Planetary Sciences*, *16*, 543–603.

Holk, G. J., Kyser, T. K., Chipley, D., Hiatt, E. E., & Marlatt, J. (2003). Mobile Pb-isotopes in Proterozoic sedimentary basins as guides for exploration of uranium deposits. *Journal of Geochemical Exploration*, *80*(2), 297–320. http://doi.org/10.1016/S0375-6742(03)00196-1

Jackson, R. G. (2010). Application of 3D geochemistry to mineral exploration. *Geochemistry: Exploration, Environment, Analysis*, *10*(2), 143–156. http://doi.org/10.1144/1467-7873/09-217

Jeanneret, P., Goncalves, P., Durand, C., Trap, P., Marquer, D., Quirt, D., & Ledru, P. (2016). Tectono-metamorphic evolution of the pre-Athabasca basement within the Wollaston–Mudjatik Transition Zone, Saskatchewan. *Canadian Journal of Earth Sciences*, *53*(3), 231–259. http://doi.org/10.1139/cjes-2015-0136

Jeanneret, P., Goncalves, P., Durand, C., Poujol, M., Trap, P., Marquer, D., Quirt, D., & Ledru, P. (2017). Geochronological constraints on the Trans-Hudsonian tectono-metamorphic evolution of the pre-Athabasca basement within the Wollaston–Mudjatik Transition Zone, Saskatchewan. *Precambrian Research*, *301*, 152–178. https://doi.org/10.1016/j.precamres.2017.07.019

Jefferson, C. W., Thomas, T. J., Gandhi, S. S., Ramaekers, P., Delaney, G., Brisbin, D., Cutts, C., Portella, P., & Olson, R.A. (2007). Unconformity-associated uranium deposits of the Athabasca Basin, Saskatchewan and Alberta. *In* Jefferson C.W. & Delaney, G. (eds.), *EXTECH IV: Geology and Uranium EXploration TECHnology of the Proterozoic Athabasca Basin, Saskatchewan and Alberta*: Geological Survey of Canada, Bulletin 588, 23–67.

Jenner, G. A. (1996). Trace element geochemistry of igneous rocks: geochemical nomenclature and analytical geochemistry. *In* Wyman, D. A. (ed.), *Trace element geochemistry of volcanic rocks: applications for massive sulphide exploration.* Geological Association of Canada. Short Course Notes, 12, 51–77.

Kerr, W. & Wallis, R. (2014). "Real-world" economics of the uranium deposits of the Athabasca Basin, northern Saskatchewan: why grade is not always king! SEG Newsletter, (99) 1, 11–15.

Kister, P., Laverret, E., Cuney, M., Vieillard, P., & Quirt, D. (2003). 3-D distribution of alteration minerals associated with unconformity-type mineralization: Anne Zone, Shea Creek deposit (Saskatchewan, Canada). *In* Cuney, M. (ed.), *Proceedings of the International Conference on Uranium Geochemistry: Nancy, France*, p. 197–200.

Kotzer, T. G., & Kyser, T. K. (1995). Petrogenesis of the Proterozoic Athabasca Basin, northern Saskatchewan, Canada, and its relation to diagenesis, hydrothermal uranium mineralization

and paleohydrogeology. *Chemical Geology*, *120*(1), 45–89. http://doi.org/10.1016/0009-2541(94)00114-N

Kyser, K. (2014). Uranium Ore Deposits, *In* Turekian, H. D., Holland, H. D., (eds.), Treatise on Geochemistry (2nd ed.): Oxford, Elsevier, v. 7, p. 489–513. http://doi.org/10.1016/B978-0-08-095975-7.01122-0

Kyser, K., & Cuney, M. (2008). Unconformity-related uranium deposits. *In* Cuney, M. & Kyser, K., (eds.), *Recent and not-so-recent developments in uranium deposits and implications for exploration*. Quebec: Mineralogical Association of Canada Short Course Series Vol. 39, 161–219. ISBN 978-0-921294-48-1

Kyser, K., Hiatt, E., Renac, C., Durocher, K., Holk, G., & Deckart, K. (2000). Diagenetic fluids in Paleo-and Meso-Proterozoic sedimentary basins and their implications for long protracted fluid histories. *In* Kyser, K. (ed.), *Fluids and basin evolution.* Mineralogical Association of Canada Short Course Series 28, 225–262. http://doi.org/10.13140/2.1.1033.1847

Lewry, J. F., & Sibbald, T. I. I. (1980). Thermotectonic evolution of the Churchill Province in northern Saskatchewan. *Tectonophysics*, *68*, 45–82.

Li, Z., Chi, G., & Bethune, K. M. (2016). The effects of basement faults on thermal convection and implications for the formation of unconformity-related uranium deposits in the Athabasca Basin, Canada. *Geofluids*, *16*(4), 729–751. http://doi.org/10.1111/gfl.12180

Macdonald, C. (1985). Mineralogy and geochemistry of the sub-Athabasca regolith near Wollaston Lake. *In* Sibbald, T. I. I. & Petruk, W. (eds.), *Geology of Uranium Deposits: Canadian Institute of Mining and Metallurgy Special Vol. 32*, 155–158.

Madore, C., Annesley, I. R., & Wheatley, K. (2000). Petrogenesis, age, and uranium fertility of peraluminous leucogranites and pegmatites of the McClean Lake/Sue and Key Lake/P-Patch deposit areas, Saskatchewan. In *GAC-MAC Program with Abstracts* (Vol. 25) No. 1041, p. 4.

McGill, B. D., Marlatt, J. L., Matthews, R. B., Sopuck, V. J., Homeniuk, L. A., & Hubregtse, J. J. (1993). The P2 north uranium deposit, Saskatchewan, Canada. *Exploration and Mining Geology*, *2*(4), 321–331.

Mercadier, J., Cuney, M., & Quirt, D. (2009). Basement-hosted uranium oxides from Athabasca Basin: mineralogy, U/Pb dating, major and Rare Earth Element (REE) concentrations: comparison with U-oxides from deposits located in the vicinity of the unconformity. *In* Lentz, D. R., Thorne, K. G., & Beal, K-L. (eds.), *Proceedings of the 24th IAGS, Fredericton, Canada*, 445–448. ISBN 978-1-55131-136-4

Mwenifumbo, C. J. & Bernius, G. R.. (2007). Crandallite-group minerals: host of thorium enrichment in the eastern Athabasca Basin, Saskatchewan. *In* Jefferson C.W. & Delaney, G. (eds.), *EXTECH IV: Geology and Uranium EXploration TECHnology of the Proterozoic Athabasca Basin, Saskatchewan and Alberta*: Geological Survey of Canada, Bulletin 588, 521–532.

Ng, R., Alexandre, P., & Kyser, K. (2013a). Mineralogical and geochemical evolution of the unconformity-related McArthur River Zone 4 orebody in the Athabasca Basin, Canada: implications of a silicified zone. *Economic Geology*, *108*(7), 1657–1689. http://doi.org/10.2113/econgeo.108.7.1657

Ng, R., Alexandre, P., Kyser, K., Cloutier, J., Abdu, Y. A., & Hawthorne, F. C. (2013b). Oxidation state of iron in alteration minerals associated with sandstone-hosted unconformity-related uranium deposits and apparently barren alteration systems in the Athabasca Basin, Canada: Implications for exploration. *Journal of Geochemical Exploration*, *130*, 22–43. http://doi.org/10.1016/j.gexplo.2013.02.009

Pascal, M., Boiron, M. C., Ansdell, K., Annesley, I. R., Kotzer, T., Jiricka, D., & Cuney, M. (2016). Fluids preserved in variably altered graphitic pelitic schists in the Dufferin Lake Zone, south-central Athabasca Basin, Canada: Implications for graphite loss and uranium deposition. *Mineralium Deposita, 51*(5), 619–636. http://doi.org/ 10.1007/s00126-015-0628-6

Pagel, M., Poty, B., & Sheppard, S. M. F. (1980). Contribution to some Saskatchewan uranium deposits mainly from fluid inclusions and isotopic data. *In* Ferguson, S. & Goleby, A. (eds.), *Uranium in the Pine Creek Geosyncline: Vienna, International Atomic Energy Agency*, p. 639–654.

Percival, J. B., & Kodama, H. (1989). Sudoite from Cigar Lake, Saskatchewan. *Canadian Mineralogist*, *27*, 633–641.

Polito, P. A., Kyser, T. K., & Stanley, C. (2009). The Proterozoic, albitite-hosted, Valhalla uranium deposit, Queensland, Australia: a description of the alteration assemblage associated with uranium mineralisation in diamond drill hole V39. *Mineralium Deposita*, *44*(1), 11–40. http://doi.org/ 10.1007/s00126-007-0162-2

Quirt, D. H. (1985). Lithogeochemistry of the Athabasca Group: Summary of sandstone data. *In* Summary of Investigations 1985, Saskatchewan Geological Survey, Saskatchewan Energy and Mines, Miscellaneous Report 85-4, p. 128–132.

Quirt, D. H. (1995). Norm calculation procedure for sandstone clay minerals. Saskatchewan Research Council, Publication No. R-1230-28-E-95, 14 p. plus appendices.

Quirt, D. H. (2001). Kaolinite and dickite in the Athabasca sandstone, northern Saskatchewan, Canada. Saskatchewan Research Council, Publication No. 10400-16D01, 27 p.

Quirt, D. (2009). Applying Pb isotopes in unconformity-type uranium exploration. *In* Lentz, D. R., Thorne, K. G., & Beal, K-L. (eds.), *Proceedings of the 24th IAGS, Fredericton, Canada*, 453–456. ISBN 978-1-55131-136-4

Quirt, D. H., & Wasyliuk, K. (1997). Kaolinite, dickite, and other clay minerals in the Athabasca Group, Canada, and the Kombolgie Formation, Australia: 11th International Clay Conference, Ottawa, Ontario, June 1997. In *Proceedings A* (Vol. 61).

Quirt, D., Kotzer, T., and Kyser, T.K. (1991). Tourmaline, phosphate minerals, zircon and pitchblende in the Athabasca Group: Maw Zone and McArthur River areas. *In* Summary of Investigations 1991: Saskatchewan Geological Survey, Saskatchewan Energy and Mines, Report 91-4, p. 181–191.

Rainbird, R. H., Stern, R. A., Rayner, N., & Jefferson, C. W. (2007). Age, provenance, and regional correlation of the Athabasca Group, Saskatchewan and Alberta, constrained by igneous and detrital zircon geochronology. *In* Jefferson C.W. & Delaney, G. (eds.), *EXTECH IV: Geology and Uranium EXploration TECHnology of the Proterozoic Athabasca Basin, Saskatchewan and Alberta*: Geological Survey of Canada, Bulletin 588, 193–209.

Ramaekers, P., & Catuneanu, O. (2004). Development and sequences of the Athabasca Basin, early Proterozoic, Saskatchewan and Alberta, Canada. *In* Eriksson P. G., Alterman, W., Nelson, D. R., Mueller, W. U., & Catuneanu, O. (eds.), *The Precambrian Earth: Tempos and Events* (Vol. 12, pp. 705–723). Amsterdam: Elsevier.

Ramaekers, P., Jefferson, C. W., Yeo, G. M., Collier, B., Long, D. G. F., Drever, G., McHardy, S., Jiricka, D., Cutts, C., Wheatley, K., Catuneanu, O., Bernier, S., Kupsch, B., & Post, R. T. (2007). Revised geological map and stratigraphy of the Athabasca Group, Saskatchewan and Alberta. *In* Jefferson C.W. & Delaney, G. (eds.), *EXTECH IV: Geology and Uranium EXploration TECHnology of the Proterozoic Athabasca Basin, Saskatchewan and Alberta*: Geological Survey of Canada, Bulletin 588, 155–187.

Reimann, C., Filzmoser, P., & Garrett, R. G. (2005). Background and threshold: critical comparison of methods of determination. *Science of the Total Environment*, *346*(1), 1–16. http://doi.org/10.1016/j.scitotenv.2004.11.023

Richard, A., Pettke, T., Cathelineau, M., Boiron, M. C., Mercadier, J., Cuney, M., & Derome, D. (2010). Brine–rock interaction in the Athabasca basement (McArthur River U deposit, Canada): consequences for fluid chemistry and uranium uptake. *Terra Nova*, *22*(4), 303–308. http://doi.org/10.1111/j.1365-3121.2010.00947.x

Roy, C., Halaburda, J., Thomas, D., & Hirsekorn, D. (2006). Millennium deposit-Basement-hosted derivative of the unconformity uranium model. In *Uranium production and raw materials for the nuclear fuel cycle-Supply and demand, economics, the environment and energy security: International Atomic Energy Agency Proceedings Series,* 111–121.

Schaubs, P., Ord, A., Annesley, I., Madore, C., Quirt, D., Thomas, D., Portella, P. (2005). A comparison of the McArthur River and Cigar Lake unconformity-related uranium deposits, Saskatchewan, Canada: insight from deformation-fluid flow models. In *STOMP - Structure, Tectonics, and Ore Mineralization Processes:* Townsville, Qld, 121.

Stanley, C. R., & Madeisky, H. E. (1994). Lithogeochemical exploration for hydrothermal ore deposits using Pearce element ratio analysis. *In* Lentz, D. R. (ed.), *Alteration and Alteration Processes Associated with Ore-forming systems*, Geological Association of Canada, Short Course Notes, (11), 193–211.

Sopuck, V. J., De Carle, A., Wray, E. M., & Cooper, B. (1983). Application of lithogeochemistry to the search for unconformity-type uranium deposits in the Athabasca Basin. *In* Cameron, E. M. (ed.), *Uranium Exploration in Athabasca Basin, Saskatchewan, Canada,* Geological Survey of Canada: Paper 82-11, 191–205.

Tremblay, L. (1982). Geology of the uranium deposits related to the sub-Athabasca unconformity, Saskatchewan, Canada. Geological Survey of Canada: Paper 81-20, 56 p.

Yeo, G. M., & Delaney, G. (2007). The Wollaston supergroup, stratigraphy and metallogeny of a Paleoproterozoic Wilson cycle in the Trans-Hudson Orogen, Saskatchewan. *In* Jefferson C.W. & Delaney, G. (eds.), *EXTECH IV: Geology and Uranium EXploration TECHnology of the Proterozoic Athabasca Basin, Saskatchewan and Alberta*: Geological Survey of Canada, Bulletin 588, 89–117.

Yeo, G., Jefferson, C.W., & Ramaekers, P. (2002). A preliminary comparison of Manitou Falls Formation stratigraphy in four Athabasca Basin deposystems, *In* Summary of Investigations 2002, Volume 2, Saskatchewan Geological Survey, Sask. Industry Resources, Misc. Rep. 2002-4.2 CD-ROM, Paper D-7, 14p.

Zhang, G., Wasyliuk, K., & Pan, Y. (2001). The characterization and quantitative analysis of clay minerals in the Athabasca Basin, Saskatchewan: Application of shortwave infrared reflectance spectroscopy. *The Canadian Mineralogist*, *39*(5), 1347–1363. http://doi.org/10.2113/gscanmin.39.5.1347

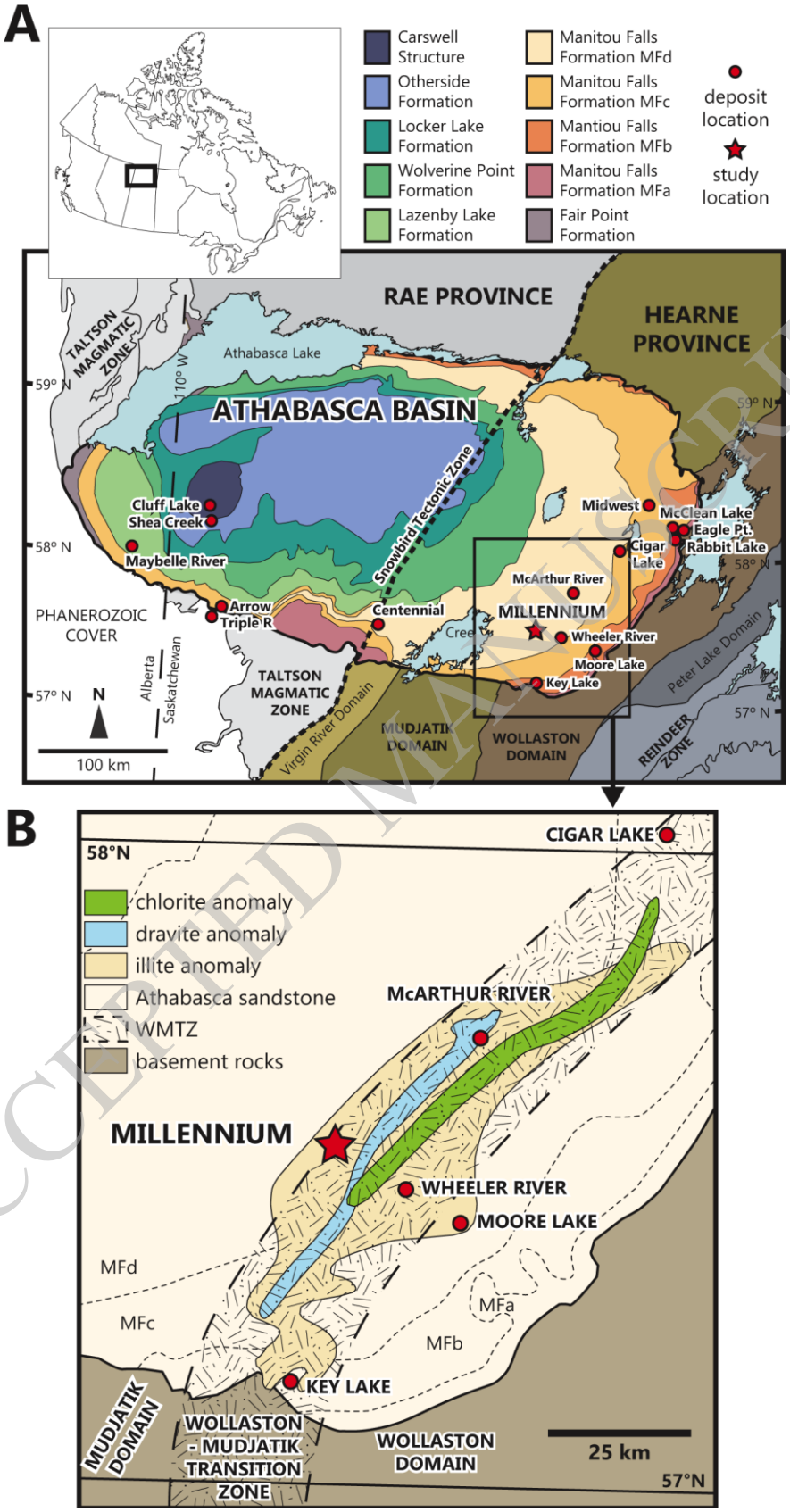

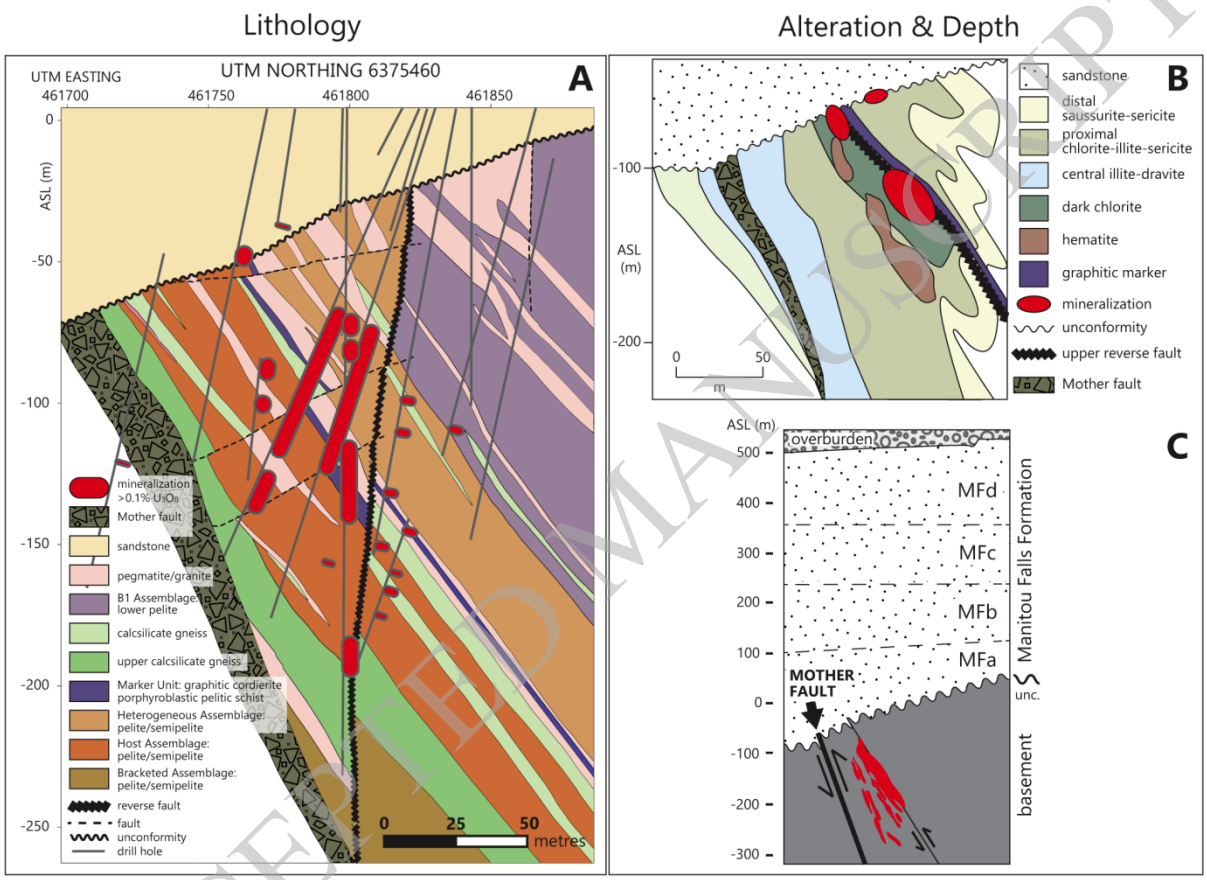

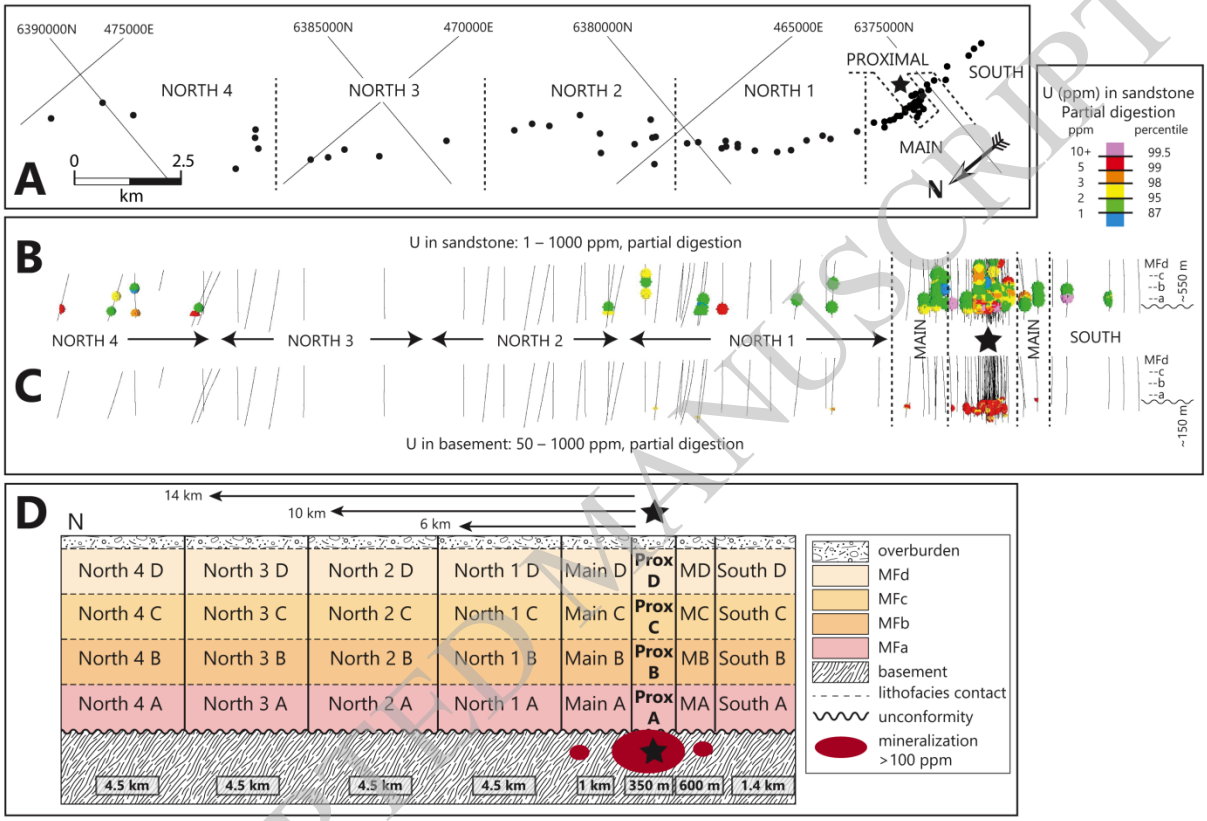

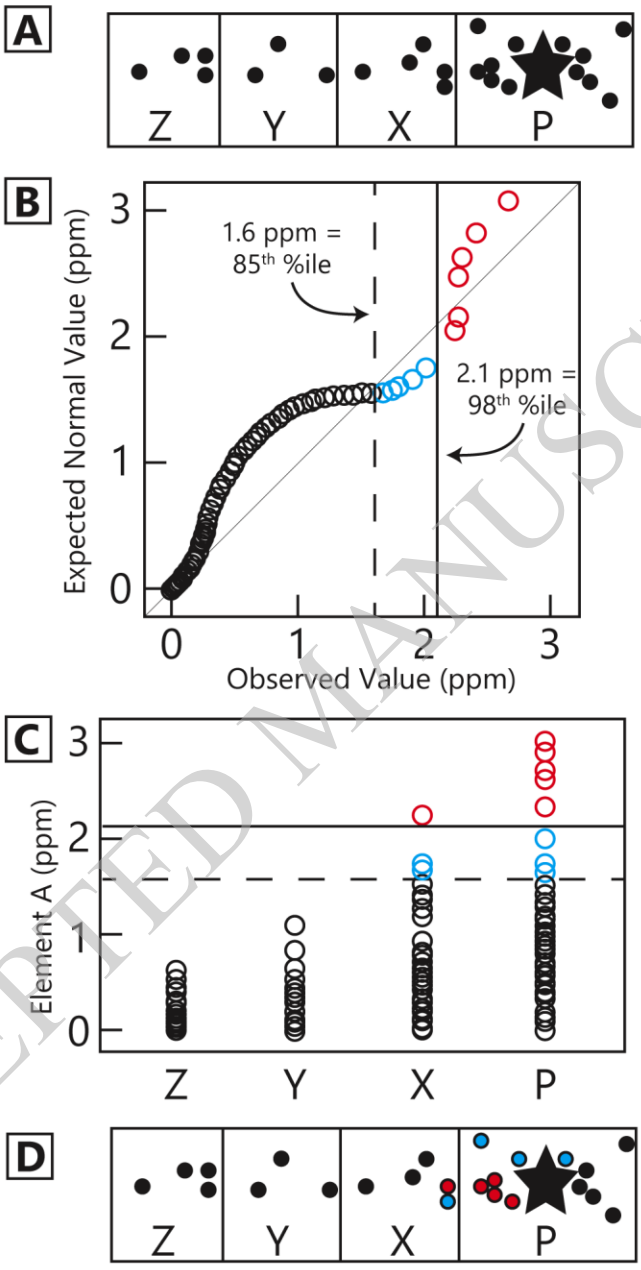

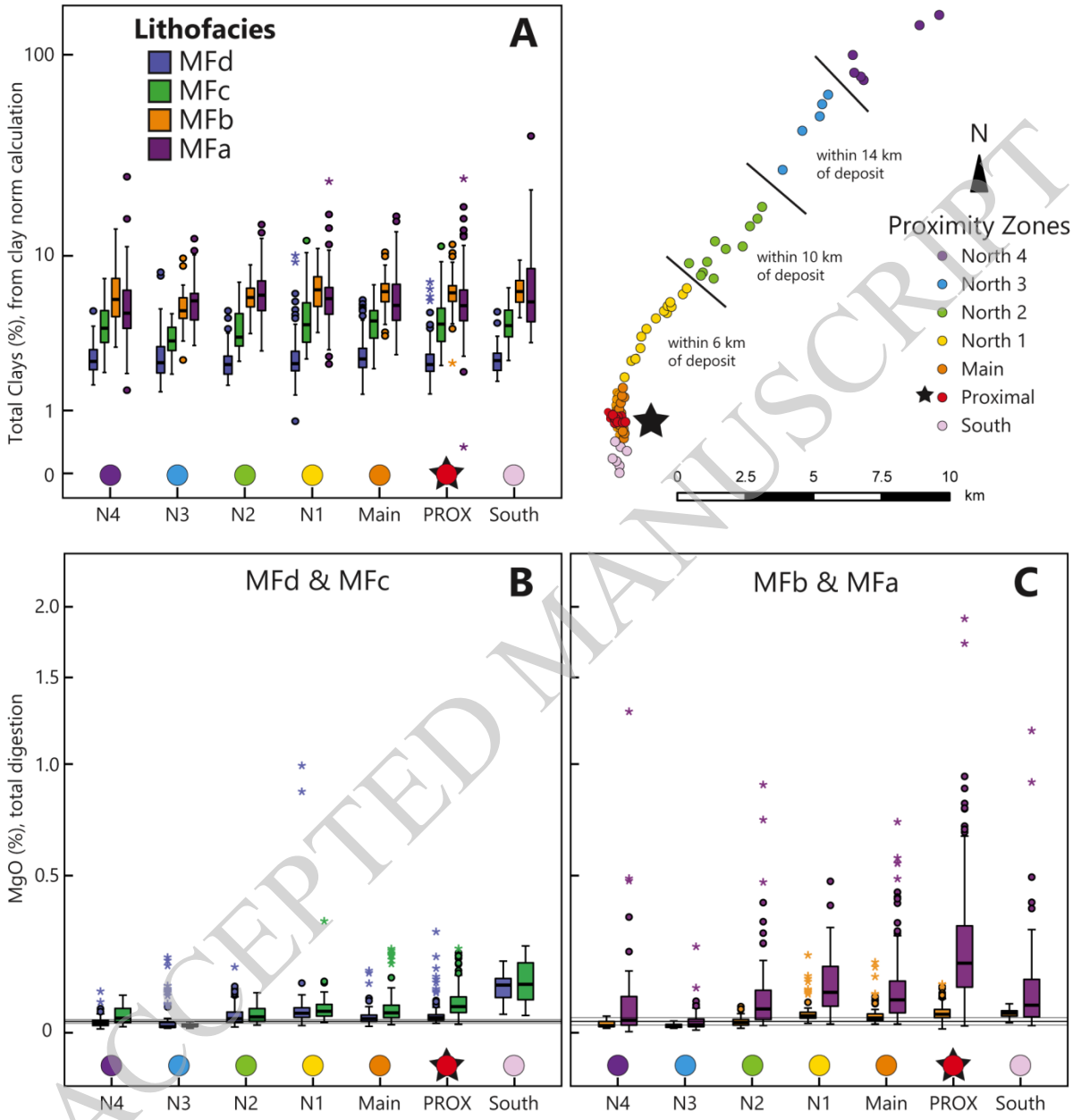

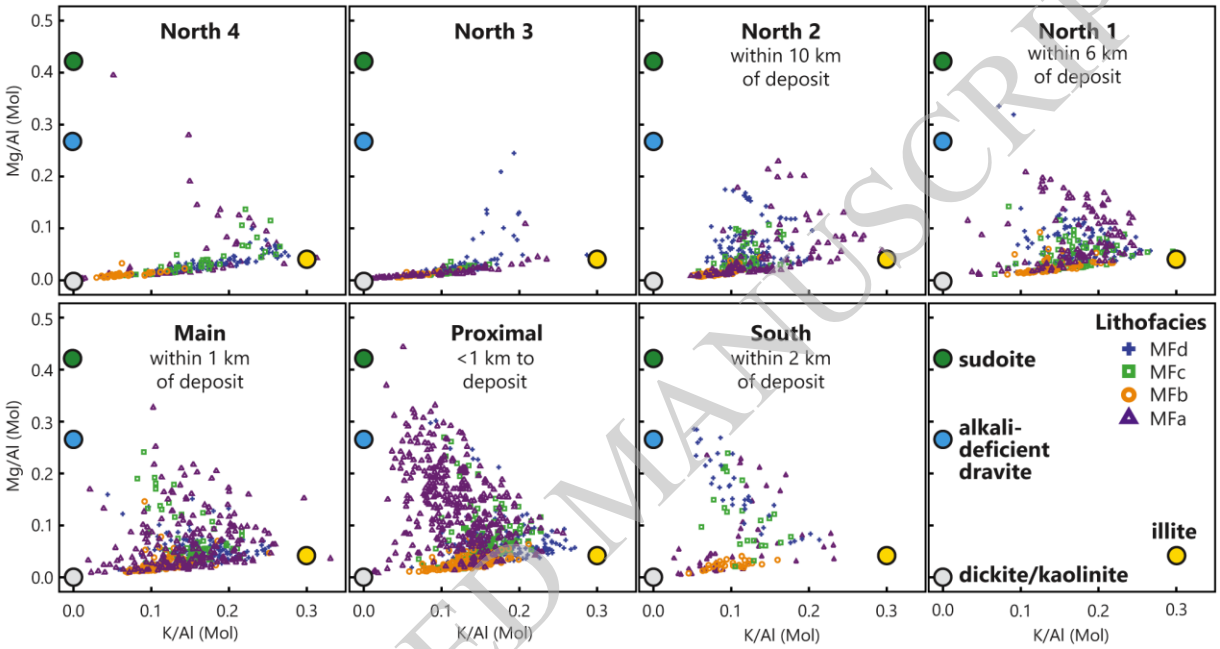

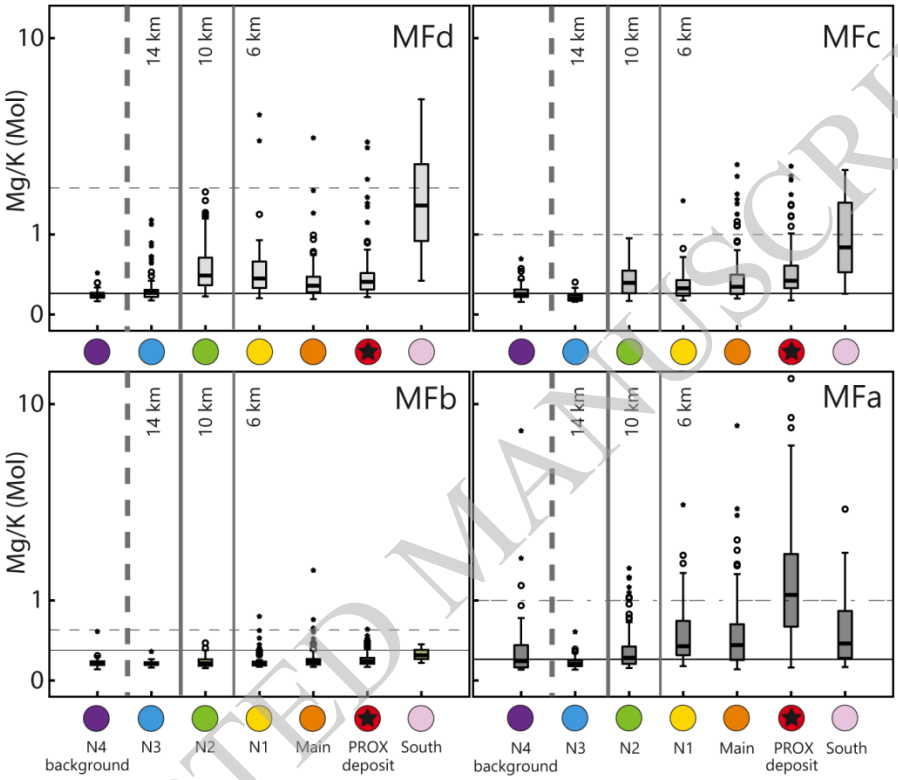

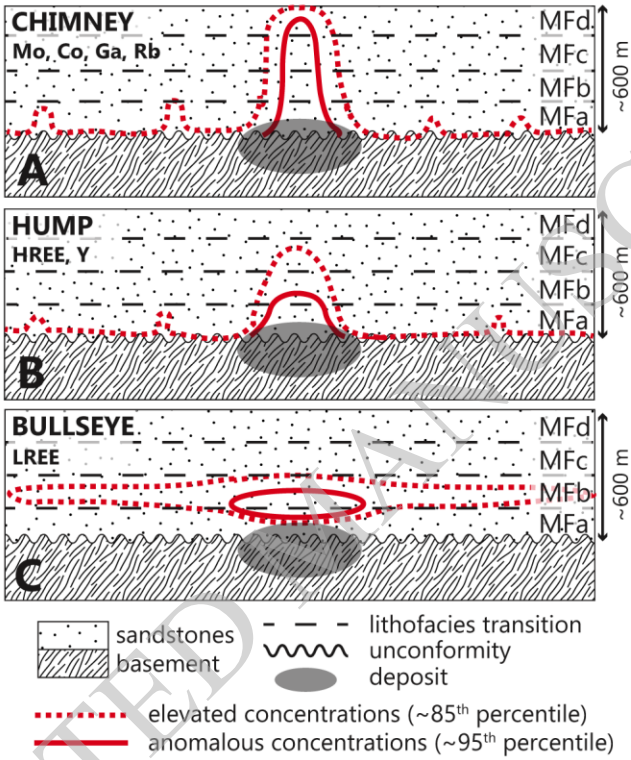

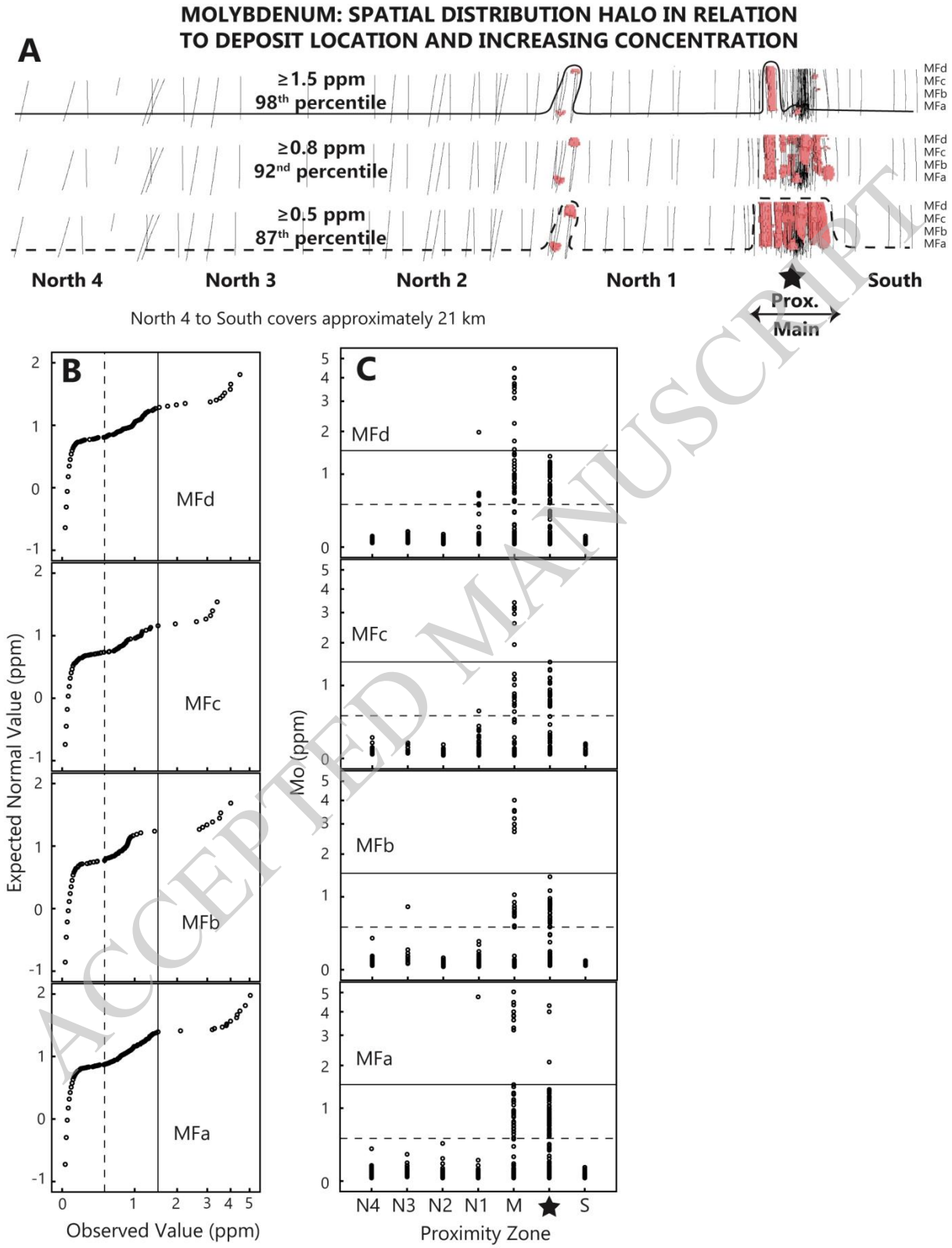

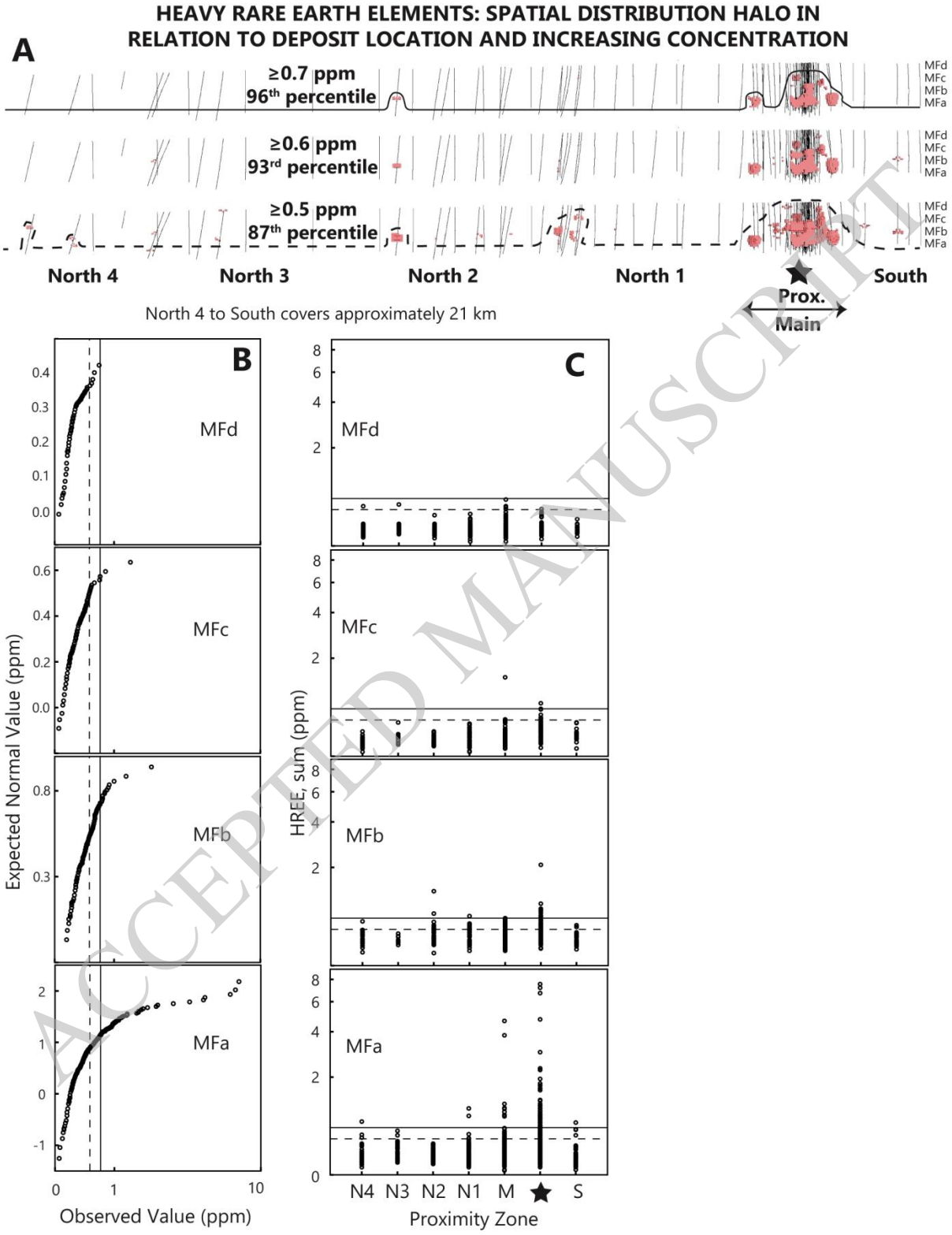

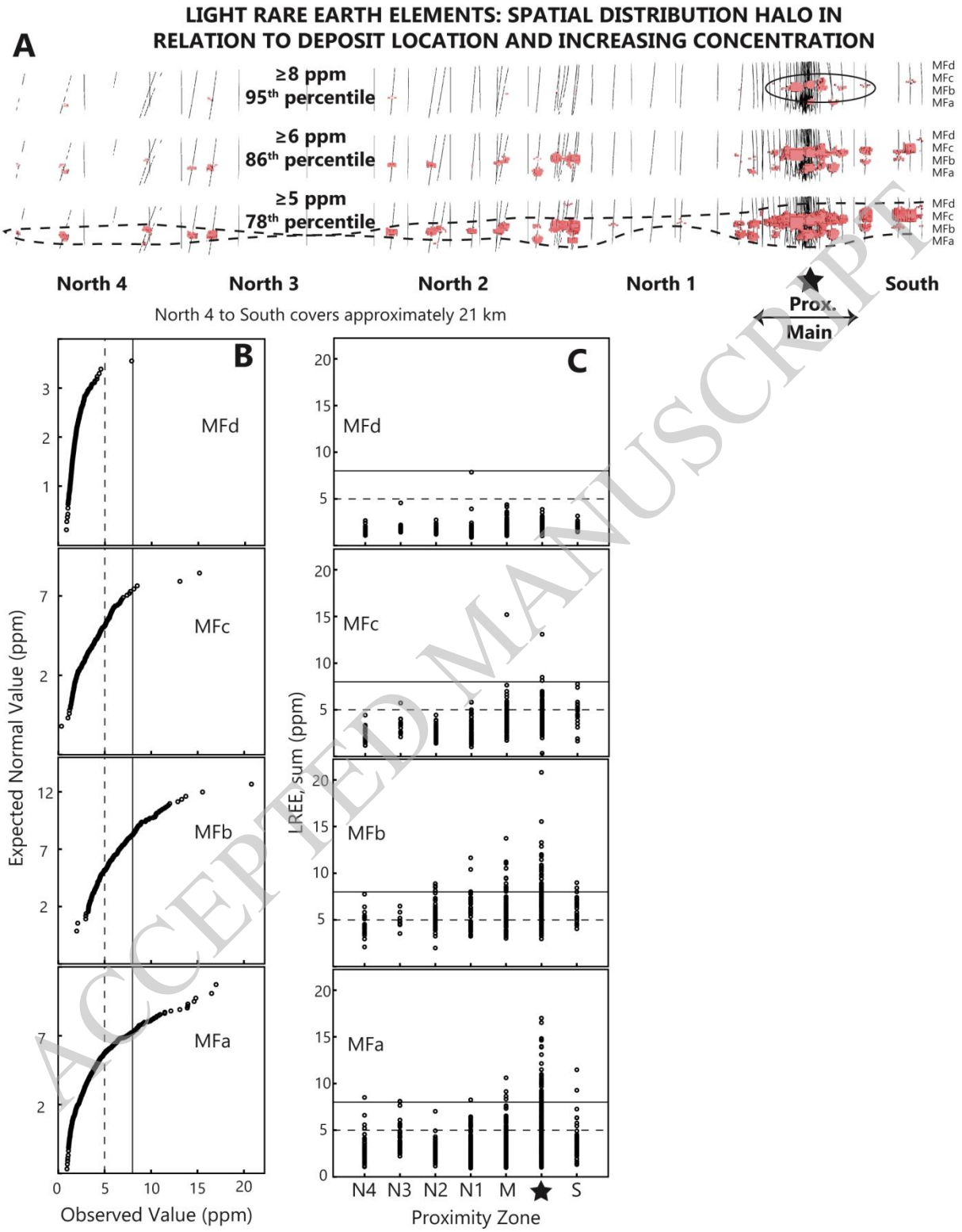

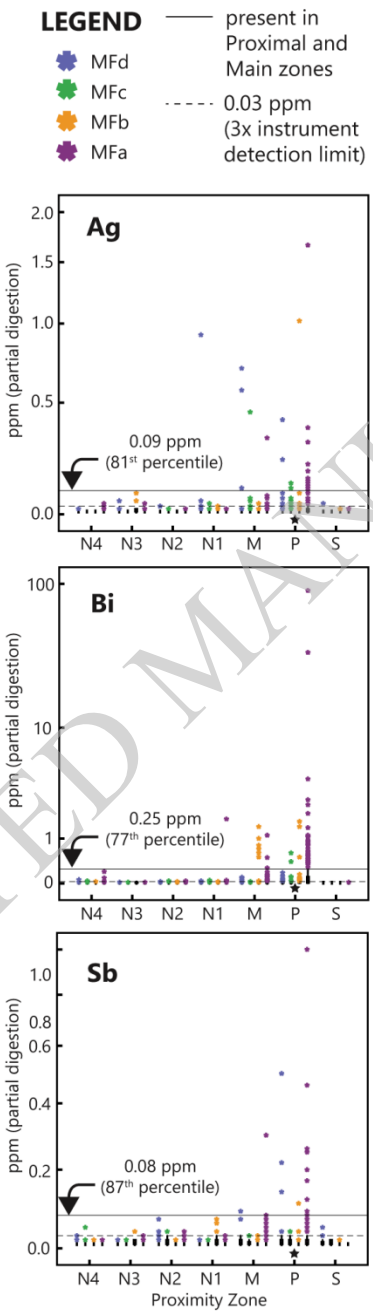

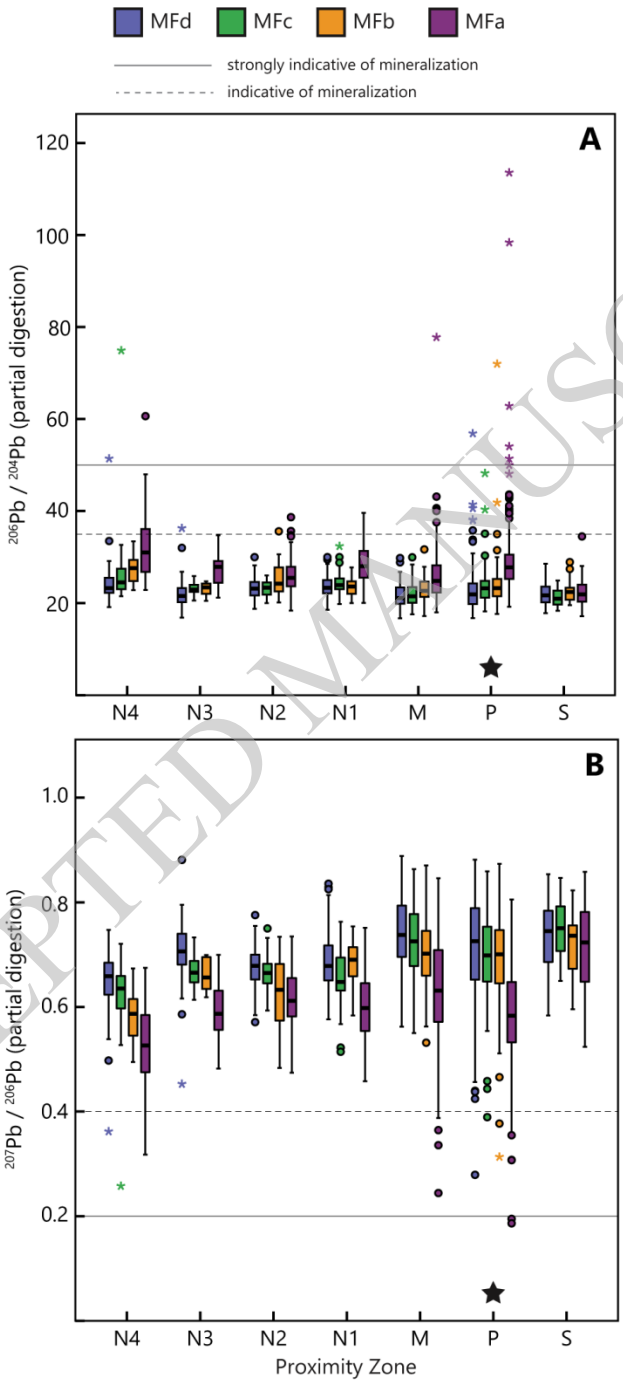

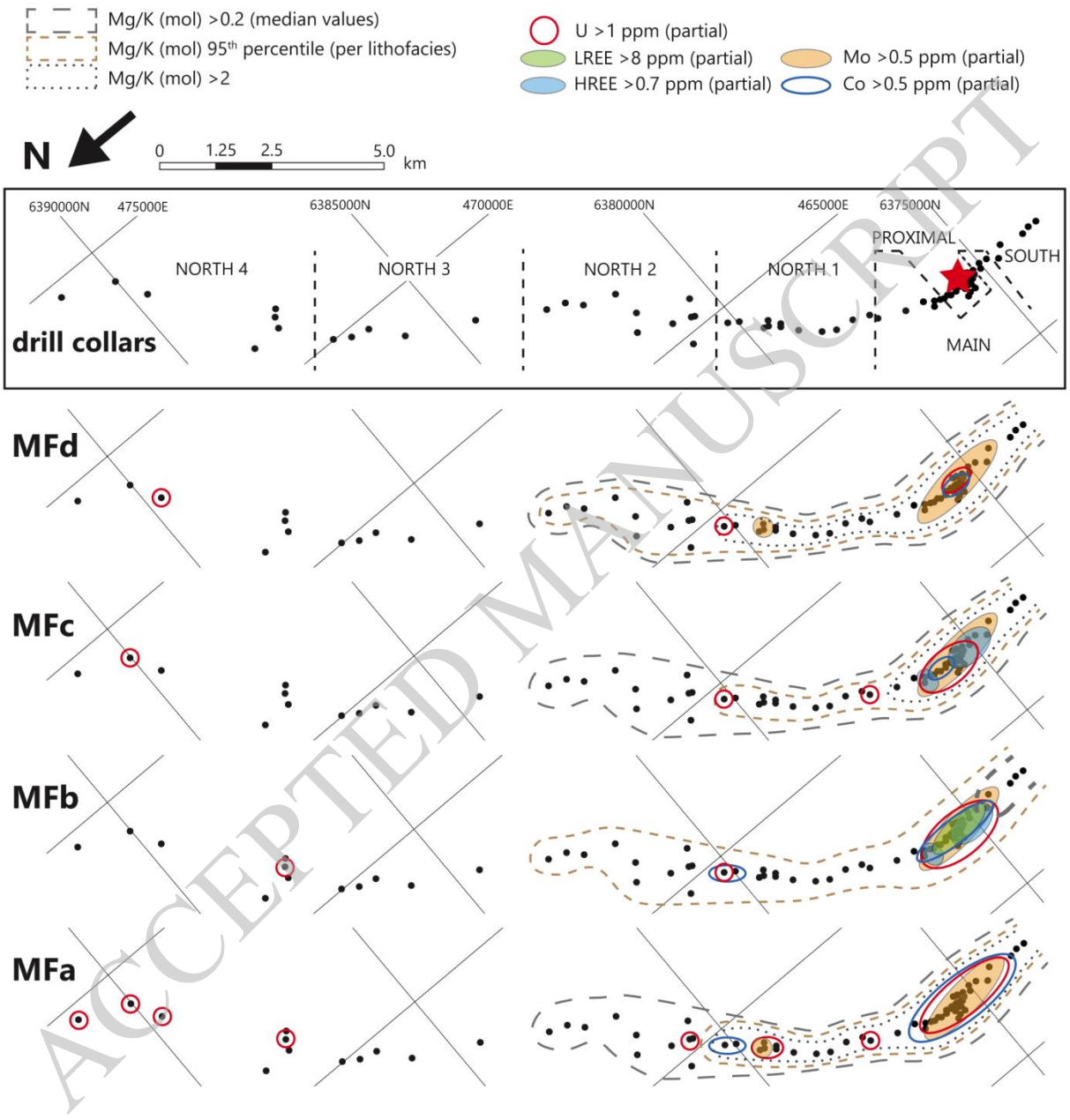

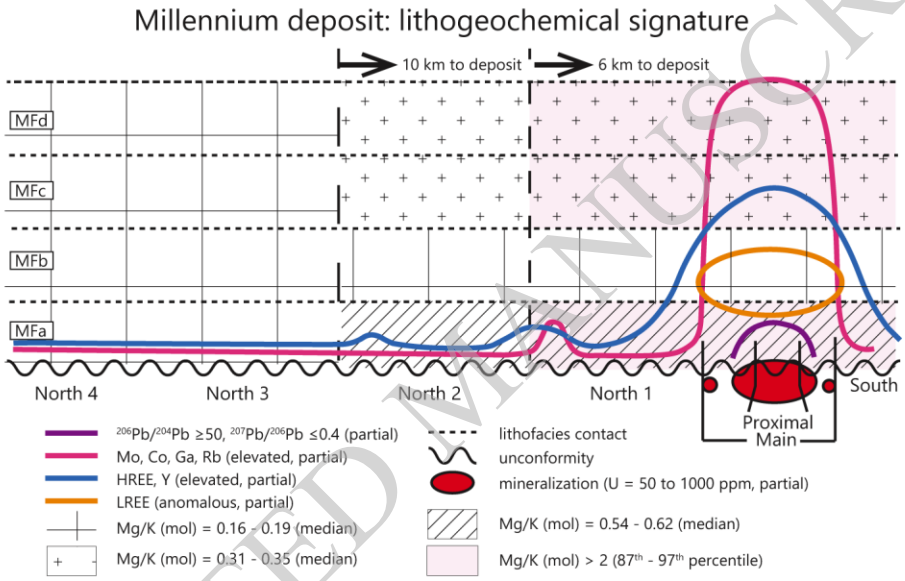

Table 1: ***Trace element haloes measured in the Proximal and Main zones above deposit***

Element	ppm partial digestion	percentile*	elevated or anom. values†	m‡ along strike	m‡ across strike	m(max)§ above unc.
U	≥50	99	anomalous	350	150	150
Pattern 1: Chimney						
Mo	≥0.3	86	elevated	1200	450	650
	≥1.0	95	anomalous	950	450	650
	≥1.5	98	anomalous	100	300	650
Co	≥0.4	87	elevated	1100	400	650
	≥0.6	95	anomalous	1000	400	650
	≥1.0	98	anomalous	1000	350	150
Ga	≥0.2	83	elevated	1700	500	650
	≥0.3	96	anomalous	1100	450	500
Rb	≥0.25	88	elevated	1700	600	650
	≥0.35	97	anomalous	1100	400	550
Ag	≥0.09	81	elevated	700	400	650
Bi	≥0.25	77	elevated	550	350	500
Sb	≥0.08	87	elevated	600	450	650
Pattern 2: Hump						
HREE (sum)	0.5	87	elevated	1100	500	650
	0.7	95	anomalous	850	400	500
Dy	≥0.4	97	anomalous	850	400	500
Er	≥0.13	94	anomalous	850	400	500
Ho	≥0.1	97	anomalous	850	450	600
Tb	≥0.08	97	anomalous	850	350	600
Yb	≥0.1	94	elevated	1500	500	650
	≥0.13	97	anomalous	850	250	400
Hf	≥0.4	94	anomalous	700	400	500
Y	≥1	90	anomalous	1550	500	650
$^{206}Pb/^{204}Pb$	≥35 (ratio)	97	anomalous	300	250	600
	≥50 (ratio)	99	anomalous	50	25	50
$^{207}Pb/^{206}Pb$	≤0.4 (ratio)	1.2	threshold	150	200	50
	≤0.2 (ratio)	0.1	anomalous	*not enough to measure in Target*		
Pattern 3: Bullseye						
LREE (sum)	6	86	elevated	1400	500	450
	8	95	anomalous	1150	350	450
Eu	≥0.1	96	elevated	700	350	450
Gd	≥1	98	anomalous	600	300	400
Nd	≥6	98	anomalous	600	300	400
Pr	≥1.8	98	anomalous	600	300	400
Sm	≥1	98	anomalous	600	300	400

* percentile values do not include data that is less than three times the instrument detection limit.
† anomalous values determined via Q-Q plots, in one or more lithofacies.
‡ halo measurements incorporate 25m cells as displayed by inverse distance weighting in Target for ArcGIS.
§ distance is measured assuming unconformity is up to 650 in depth, utilizing Target for ArcGIS in Z direction.